ELECTRONIC PROPERTIES OF DEEP-LEVEL DEFECTS IN PROTON IRRADIATED AlGaAs-GaAs SOLAR CELLS

Sheng S. Li
Department of Electrical Engineering
University of Florida
Gainesville, FL 32611

September 1981

NASA Grant No. NSG 1425
FINAL REPORT
For period September 1, 1977 through August 31, 1981

Sponsored by

NATIONAL AERONAUTICS AND SPACE ADMINISTRATION
Langley Research Center
Hampton, Virginia 23665

TECHNICAL REPORT STANDARD TITLE PAGE

1. Report No.	2. Government Accession No.	3. Recipient's Catalog No.

4. Title and Subtitle	5. Report Date
Electronic properties of deep-level defects in proton irradiated AlGaAs-GaAs solar cells.	September 1981
	6. Performing Organization Code
7. Author(s) Sheng S. Li	8. Performing Organization Report No.
9. Performing Organization Name and Address University of Florida Gainesville, FL 32611	10. Work Unit No.
	11. Contract or Grant No. NSG-1425
	13. Type of Report and Period Covered Final Report Sept. 1, 1977 - Aug. 31, 1981.
12. Sponsoring Agency Name and Address National Aeronautics and Space Administration Langley Research Center Hampton, Virginia 23665	14. Sponsoring Agency Code

15. Supplementary Notes

16. Abstract

17. Key Words (Selected by Author(s))	18. Distribution Statement
AlGaAs-GaAs solar cell, proton irradiation, deep-level defects, periodic thermal annealing, DLTS, I-V, C-V, SEM-EBIC, Diffusion length, Damage Constant.	

19. Security Classif. (of this report)	20. Security Classif. (of this page)	21. No. of Pages	22. Price*
Unclassified.	Unclassified.		

*For sale by the Clearinghouse for Federal Scientific and Technical Information, Springfield, Virginia 22151.

ABSTRACT

This final report summarizes the major technical findings made in the research program at the University of Florida sponsored by NASA Langley Research Center under grant No. NSG-1425 during the period from September 1, 1977 through August 31, 1981. The main objective of this research program is to obtain detailed information concerning the electronic properties of radiation induced deep-level defects and their influence on the performance of the proton irradiated GaAs solar cells. Characterization of these defects by the Deep-Level Transient Spectroscopy (DLTS) and Capacitance-Voltage (C-V) techniques as well as analyzing the forward current-voltage (I-V) characteristics and SEM-EBIC data have been carried out in this work for the proton irradiated GaAs solar cells over a wide range of proton energies (i.e., 50, 100, 200, 290, 800 KeV, 1 and 10 MeV) and proton fluences (i.e., 10^{10}, 10^{11}, 5×10^{11}, 10^{12}, and 10^{13} P/cm^2). Important defect and recombination parameters such as defect energy levels and density, carrier capture cross sections and lifetimes as well as diffusion lengths in the undoped n-GaAs LPE layers have been determined in this work. Good correlation between these defect parameters and solar cell performance parameters (V_{oc}, J_{sc}, and η_c) has also been obtained for GaAs solar cells irradiated by 200 and 290 KeV protons. From this study, it was found that 200 to 290 KeV protons will produce the most defects and damages to the GaAs solar cell structure used in this study. Thus, a detailed study has been conducted to investigate the influence of the low temperature (200 to 400° C) periodic thermal annealing on the deep-level defects and the performance of the 200 KeV proton irradiated solar Cells. The results of this study are discussed in this report. Most of the proton induced defects found in this study are attributed to vacancy or antisite related defects and can be effectively annealed out by low temperature annealing process. Damage coefficients for low energy protons ($E_p \leq 300$ KeV) deduced from hole diffusion lengths were found to vary between 1 and 2×10^{-4}.

TABLE OF CONTENTS

I. INTRODUCTION AND SUMMARY

The objectives of this research program are: (1) to study the electronic properties of deep-level defects induced by proton irradiation in AlGaAs-GaAs solar cells; (2) to understand the basic recombination mechanisms associated with these deep-level defects; (3) to correlate the measured defect and recombination parameters with the solar cell performance parameters such as open circuit voltage and short circuit current, and (4) to study the effect of low temperature (200 to 400° C) thermal annealing process on the deep-level defects and the dark I-V characteristics in the AlGaAs-GaAs solar cells irradiated by 200 KeV protons of 10^{11} P/cm^2 proton fluence. Technical findings in conjunction with this study goal have been given in our previous NASA technical reports [1-3] as well as in our published journal and conference papers [4-13]. In this report, highlights of the results of our previous study on the I-V, C-V, and DLTS measurements versus proton energies (100, 200, 290, 800 KeV and 10 MeV) and proton fluences (10^{10}, 10^{11}, 10^{12}, and 10^{13} cm^{-2}) are given in this report. Detailed description of the results of our current study on the influence of low temperature periodic thermal annealing process (up to four cycles) on the deep-level defects and the I-V characteristics in the 200 KeV proton irradiated AlGaAs-GaAs solar cells will be given in this report.

Among all the proton energies studied, we have found that 200 to 290 KeV protons will produce the most damage and generate more defects in the AlGaAs-GaAs solar cells than other proton energies. This is due to the fact that 200 to 290 KeV protons penetrate 1 to 2 μm into the GaAs cell which produces the most damages and defects in the active region of the cell structure used in this study. Thus, a detailed study of the radiation induced defects and dark I-V characteristics in the 200 KeV proton irradiated AlGaAs-GaAs solar cells has been carried out in this research program, and means of reducing deep-level defects induced by the proton irradiation have also been studied. In this report, we shall describe the results

of our study on the influence of low temperature periodic thermal annealing process on the deep-level defects in the 200 KeV proton irradiated GaAs solar cells. The GaAs solar cells were first subjected to 200 KeV proton irradiation with proton fluence of 10^{11} cm^{-2} and subsequently to isothermal annealing (at 200° C, 300° C, and 400° C). We performed four cycles of periodic thermal annealing and irradiation experiments in this study. The deep-level defects and dark I-V characteristics were measured and analyzed in each irradiation and annealing cycle. Details of the study are discussed in this report.

II. FABRICATION OF GaAs SOLAR CELLS FOR PROTON IRRADIATION STUDY

2.1 Fabrication and Structure of GaAs Mesa Diodes

The GaAs mesa diodes used in this study were fabricated by Dr. R. Y. Loo at Hughes Research Laboratories (HRL), using infinite solution-melt liquid phase epitaxial technique. Fig. 2.1 shows the physical structure and the dimensions of the GaAlAs-GaAs mesa diode. The wide bandgap $Al_{.95}Ga_{.05}As$ epi-layer was used as a window layer to reduce the surface recombination at the p-GaAs surface; the p-n junction (GaAs) was formed by "Be" diffusion. The thickness of window layer and p^+GaAs layer was around 0.5 μm, and the undoped n-GaAs LPE layer was around 10 μm. The P^+-ohmic contact was formed by using Au-Zn-Ag, and the n^+-ohmic contact was formed by using Au-Ge-Ni-Ag metals. The diode area was 5.86×10^{-4} cm^2 and the mesa structure was used to reduce the surface leakage in the diode. The fabrication processes and junction structure for these mesa diodes were identical to the large area (2x2 cm^2) GaAs solar cells fabricated at HRL for space applications. This is important since it allows us to compare our measured defect parameters with the solar cell performance parameters in the proton irradiated GaAs solar cells.

2.2 Proton Irradiation Procedure

The low energy (i.e., 50 to 290 KeV) proton irradiation was performed at HRL using hydrogen implantation. The medium-energy (0.8 to 10 MeV) proton irradiation

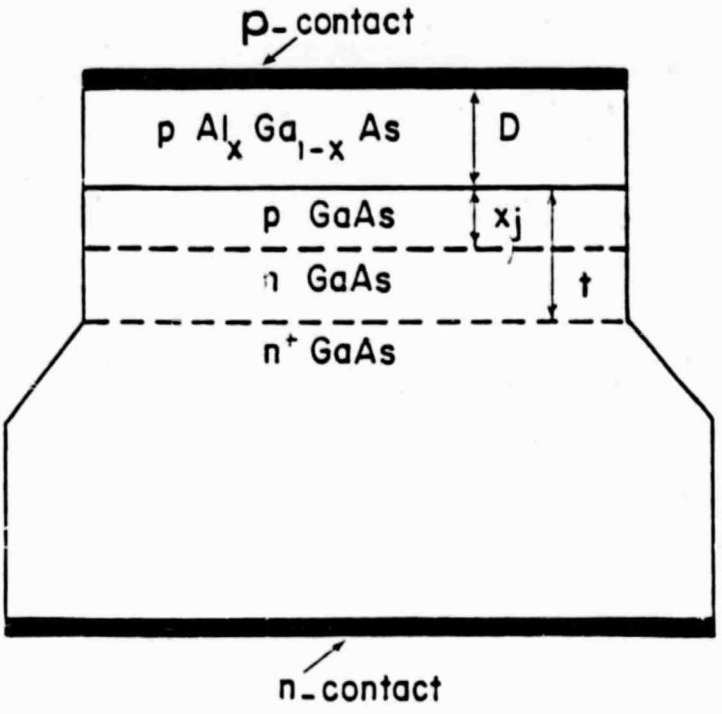

p GaAs $= 10^{18}$ cm^{-3} (Be)

n GaAs $= 10^{17}$ cm^{-3} (Sn)

n^+ GaAs $= 10^{18}$ cm^{-3} (Te)

$D < 0.5\ \mu m$

$x_j \leqslant 0.5\ \mu m$

$t > 10\ \mu m$

p contact : Au - Zn - Ag

n contact Au - Ge - Ni - Ag

p $Al_x\ Ga_{1-x}\ As$: $x = 0.95$

diode area : 5.86×10^{-4} cm^2

Fig. 2.1 (AlGa)As - GaAs Mesa diode structure used in study of the proton irradiation induced defects.

done at Caltec using their tandem accelerator. For low energy protons, the penetration depths were 0.5 μm for 50 KeV, 1 μm for 100 KeV, 1.8 μm for 200 KeV, 2.5 μm for 290 KeV, and over 10 μm for the 10 MeV protons. Thus, it is expected that proton energies between 200 and 300 KeV would create the most damage and generate more defects in the cells since these protons were stopped inside the active region (i.e., one diffusion length from junction) in the undoped n-GaAs LPE layer. Fig. 2.2 shows the proton penetration depth vs. proton energy for $E_p < 300$ KeV.

2.3 Periodic Thermal Annealing Process

In our previous NASA semiannual technical report [2] we have shown that a one-hour 300 °C thermal annealing in vacuum for the 200 KeV proton irradiated GaAs solar cells can result in a substantial reduction of the defect density. Thus, in the current research period we have focussed our efforts on the study of the influence of low temperature periodic thermal annealing (i.e., 200 to 400° C) process on the deep-level defects and the recombination current of the 200 KeV proton irradiated samples. In the periodic thermal annealing study, we limit our experiments to the simple proton energy of 200 KeV and a fluence of $1x10^{11}$ p/cm^2 for the reason cited above. The choice of 200 KeV for the proton energy represents the worst case of proton damage in these GaAs solar cells. As far as proton fluence is concerned, the 10^{11} P/cm^2 also represents the worst case in the geosynchronous orbit. The GaAs solar cells were first subjected to the 200 KeV proton irradiation ($\phi_p = 10^{11}$ P/cm^2) and subsequently to isothermal annealings at 200° C for 24 hours, 300° C for 6 hours and 400° C for 6 hours, respectively. Up to four irradiation and annealing cycles were done on these samples, and the cumulative proton fluence at the end of the fourth irradiation cycle was $4x10^{11}$ P/cm^2. Our deep-level transient spectroscopy (DLTS) measurements on these annealed samples showed that the defect density decreases nearly linearly with increasing annealing temperature, and the shallower traps were more easily to anneal out than the deeper level traps, as

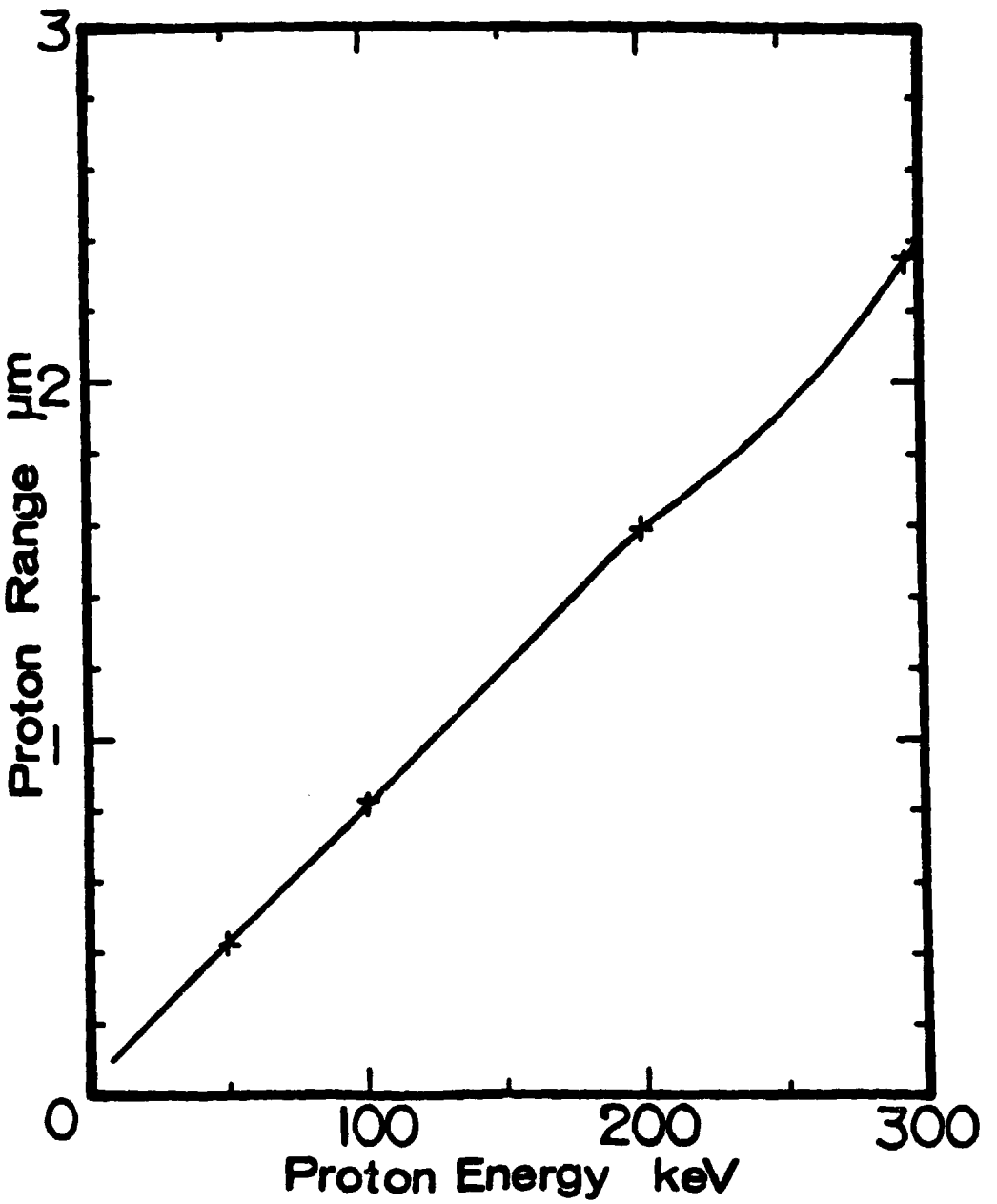

FIG. 2.2. PROTON ENERGY VERSUS PROJECTED RANGE IN GaAs.

will be discussed later.

2.4 Measurements Techniques (Diagnostic Tools)

In order to determine the defect and recombination parameters (i.e., defect density and energy levels, capture cross sections, lifetimes, and diffusion lengths) in the proton irradiated GaAs solar cells, we have performed the I-V, C-V, DLTS and SEM-EBIC measurements in these samples. Details of these measurement techniques and theories for each experiment have been described in our previous NASA technical reports [1-3] and will not be further elaborated here. In brief, the forward I-V measurements would allow us to identify the dominant current component in the solar cells under dark conditions and to evaluate the effective lifetimes in the junction space charge region of the cells [1-3]. The DLTS and C-V measurements would enable us to determine the defect parameters such as defect density and profile, energy levels, capture cross sections and carrier lifetimes as well as background dopant concentration. Fig. 2.3 shows the experimental set-up for the DLTS and C-V measurements. The SEM-EBIC measurement techniques (see Fig. 2.4 and Fig. 2.5) would provide us with a direct means for determining the minority carrier diffusion length (i.e., hole diffusion length) in n-GaAs LPE layers [1-3]. Thus, by combining the I-V, C-V, DLTS, and SEM-EBIC experiments, we can determine both the defect and recombination parameters in the proton irradiated GaAs solar cells, and enable us to correlate the measured defect parameters with the performance parameters of the large area solar cells.

III. DEFECTS PRODUCED BY PROTON IRRADIATION IN GaAs SOLAR CELLS

3.1 General Description of Defects in GaAs

In this section we shall briefly review some possible native defects resulting from vacancies, antisites, and interstitials in GaAs, while impurity related defects will not be considered here. We believe that proton irradiation induced defects are primarily due to the creation of vacancies, antisites, interstitials or complexes

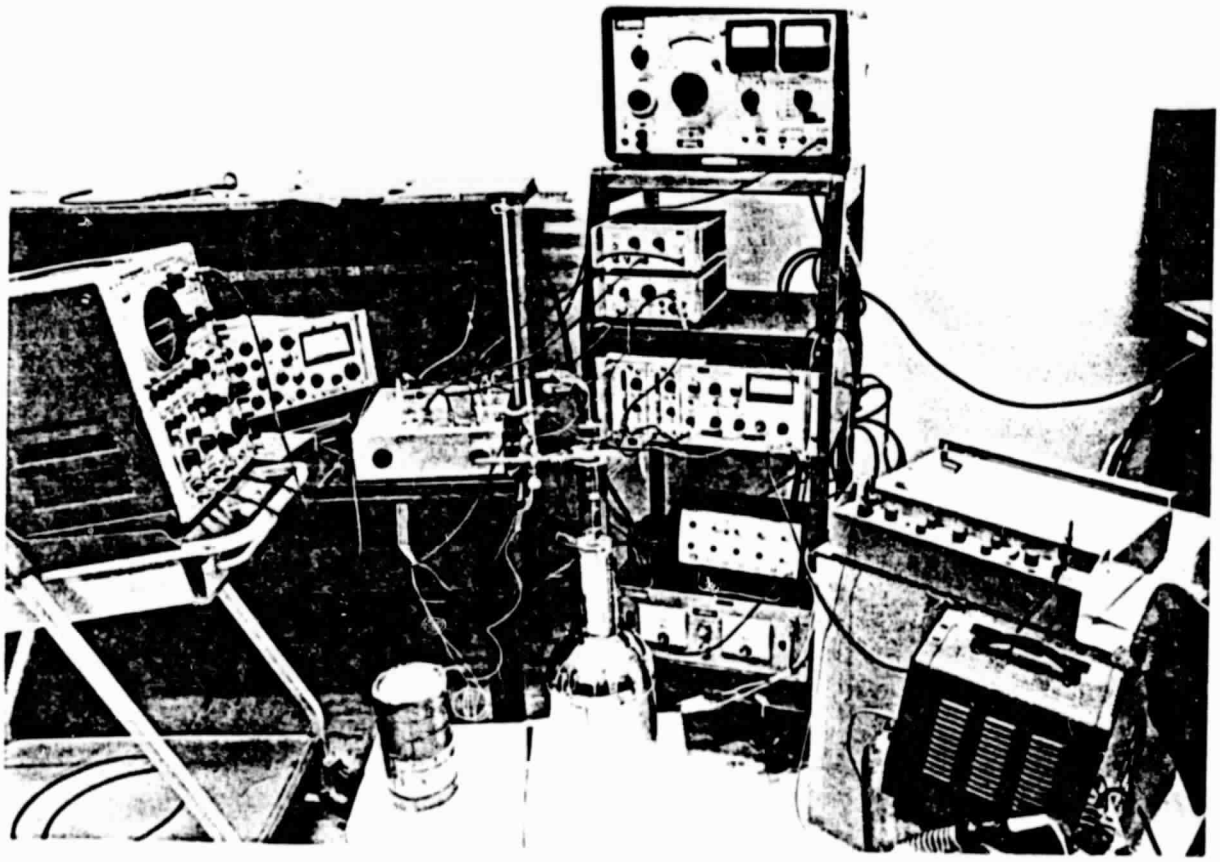

Fig. 2.3 Experimental set up for Deep Level Transient Spectroscopy (DLTS) measurement

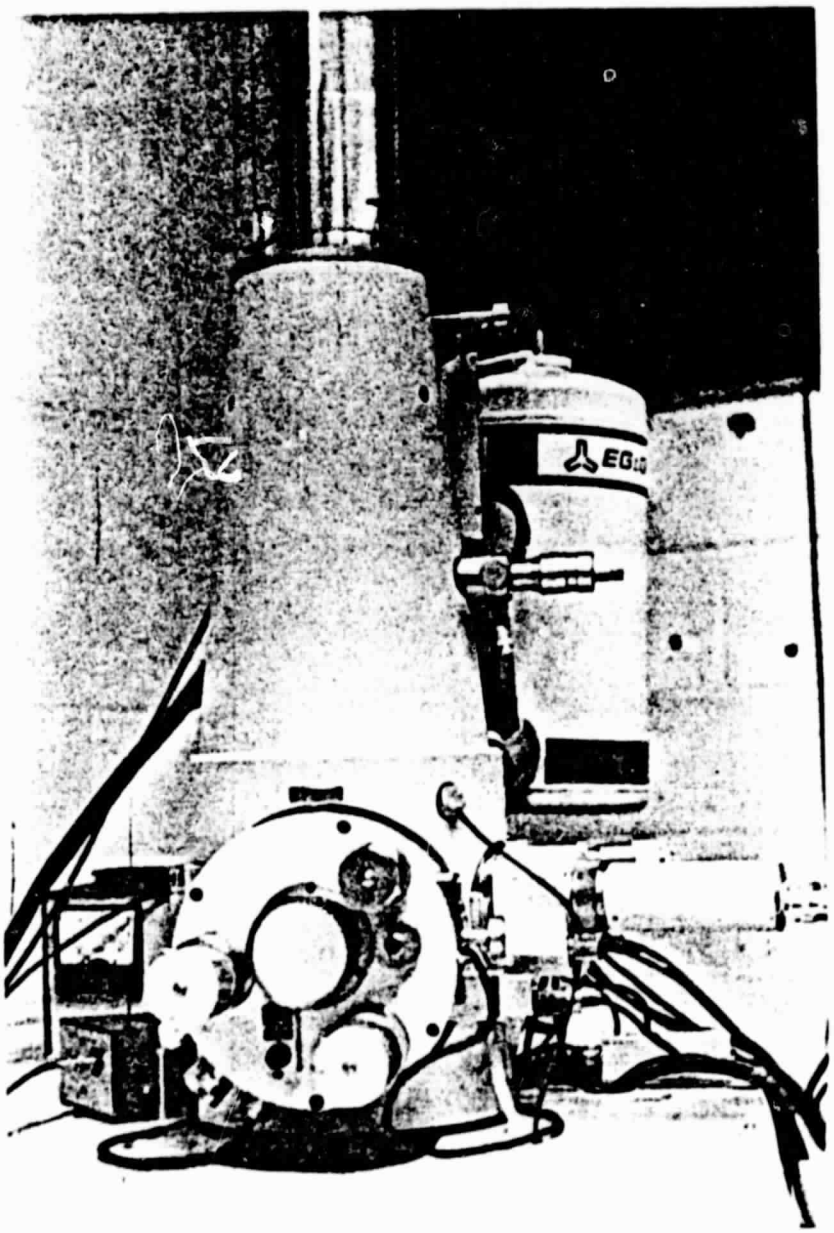

Fig. 2.4 Photograph of a JEOL-35C SEM Specimen Chamber and Vacumn Column

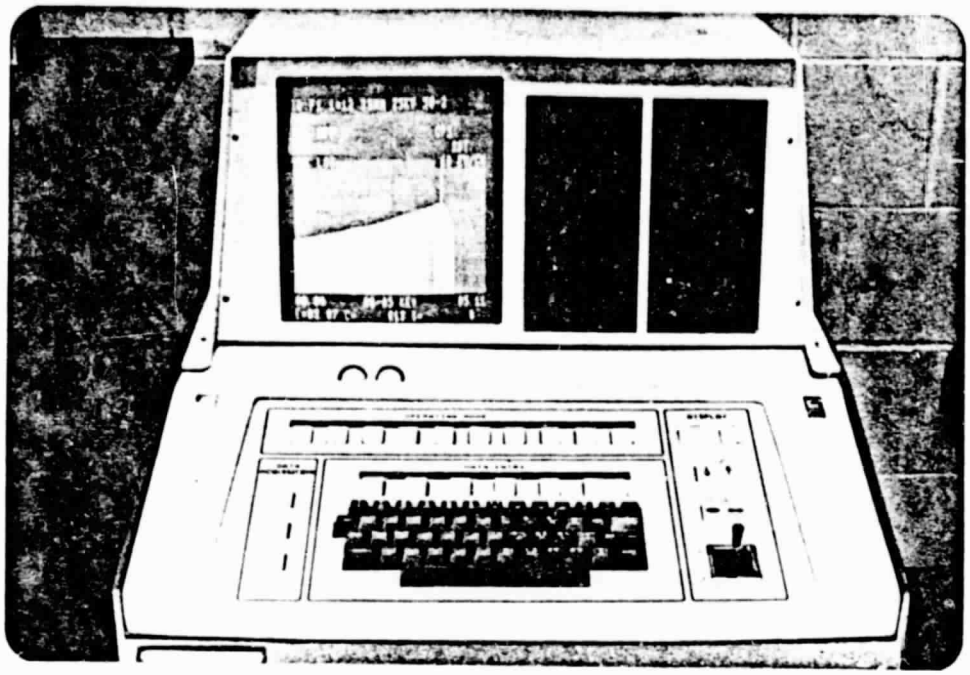

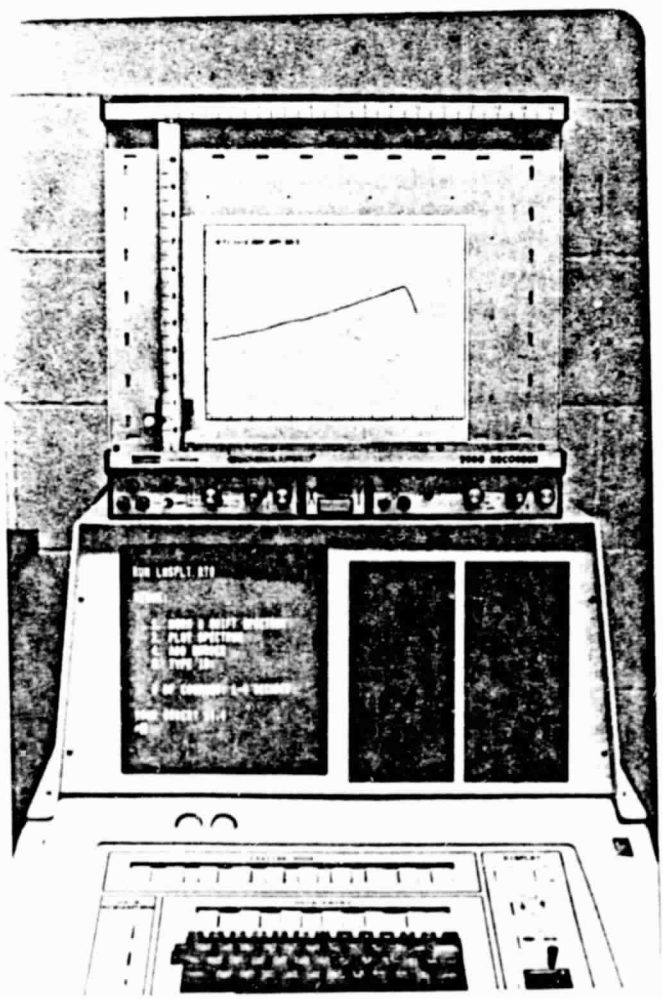

Fig. 2.5 SEM-EBIC curve displayed on an x-y recorder and the EEDS-II system

of impurity atoms (such as shallow donors) with these defects. Table 3.1 lists some possible native defects in GaAs [70]. The subscript indicates the lattice site where i stands for interstitial. "V" stands for vacancies, and V_A is a vacancy at an "A" site; A_i being "A" atom at an interstitial site. Note that the three component defects such as $V_{Ga}\ V_{As}\ V_{Ga}$ and $V_{Ga}\ As_{Ga}\ V_{Ga}$ etc. are not listed in table 3.1. Thus, it is obvious from table 2.1 that defects in GaAs and other III-v compounds are very complicated and the control of these native defects are nearly impossible. An important factor to consider in these defects is the charge states of the defect. The charge states for these native defects are important, since some of these defects formed deep electron and hole traps. These deep traps may act as recombination centers which will control the minority carrier lifetimes in the solar cells or other semiconductor devices. Thus, a brief discussion of the charge states in some of the defects listed in table 2.1 is useful in order to understand the recombination process in the proton irradiated GaAs solar cells. For examples, the gallium vacancy, "V_{Ga}^{x}," is considered as an acceptor and in neutral charge states in its normal condition; it becomes negatively charged, "V_{Ga}^{-}," when it accepts an electron. The arsenic vacancy (or vacancy complex) "V_{As}^{x}" (zero charge) is considered to be a donor that is capable of shedding an electron to become postively charged arsenic vacancy, "V_{As}^{+}." The charge states for antisities are As_{Ga}^{+2} (arsenic-gallium antisite has two positive charges), Ga_{As}^{-2} (gallium-arsenic antisite has two negative charges) and the bound pairs of these, $As_{Ga}\ Ga_{As}$, which consitute a neutral defect. Based on the quantum dielectric theory and those of Pauling's theory of electronegativities, the formation energy of GaAs antisite are given by 0.70 and 0.72 eV, respectively. This energy is much less than the energies of formation of vacancies or interstitials, and implies that antisite defects are easier to form in GaAs and can present with substantial concentrations. Indeed, the high concentrations of antisite defects have been

Table 3.1 Possible Native Defects in GaAs [70]

Gallium Vacancies Involved	Arsenic Vacancies Involved	Antisite Defects	Interstitials Involved
V_{Ga}	V_{As}	Ga_{As}	Ga_i
$(V_{Ga}\ V_{Ga})$	$(V_{As}\ V_{As})$	As_{Ga}	As_i
$(V_{Ga}\ V_{As})$	$(V_{Ga}\ V_{As})$	-	$(Ga_i\ As_i)$
-	-	$(Ga_{As}\ As_{Ga})$	-
$(Ga_i\ V_{Ga})$	-	-	$(Ga_i\ V_{Ga})$
	$(As_i\ V_{As})$	-	$(As_i\ V_{As})$
$(Ga_{As}\ V_{Ga})$	-	$(Ga_{As}\ V_{Ga})$	-
-	$(Ga_{As}\ V_{As})$	$(Ga_{As}\ V_{As})$	-
$(As_{Ga}\ V_{Ga})$	-	$(As_{Ga}\ V_{Ga})$	-
-	$(As_{Ga}\ V_{As})$	$(As_{Ga}\ V_{Ga})$	-
-	$(Ga_i\ V_{As})$	-	$(Ga_i\ V_{As})$
$(As_i\ V_{Ga})$	-	-	$(As_i\ V_{Ga})$

The Subscript indicates the lattice site where i stands for interstitial "V" denotes vacancy.

identified by infrared absorption and are inferred from EPR and other experiments [70]. Photoluminescence experimental data on GaAs reported by Chang et al have yielded luminescence peaks of 1.35, 0.81 and 0.51 eV as possible "V_{Ga}" defect levels, and 1.40 eV as "V_{As}." In general it has been found that the energy of formation of defects in GaAs has been ranked as $U_{Ga_i} > U_{V_{As}} > U_{V_{Ga}} > U_{As_i}$ [70]. A unified defect model for interface states and Schottky barriers for GaAs proposed by Spicer et al [72] have shown that the E_c-0.75 eV acceptor level was due to the missing arsenic while E_v+0.5 eV ($\pm$ 0.1 eV) donor level was attributed to the missing gallium.

In the GaAs liquid phase epitaxial layer grown from a Ga melt, normally results in two minority carrier (hole) traps in the n-type GaAs LPE layers. These hole traps termed "A" and "B" centers are at E_v+0.41 eV and E_v+0.71 eV, respectively. Recent report by Zou [70] has concluded that "A" center might be due to Ga_{As} V_{Ga} complex and "B" center might be As_{Ga} V_{Ga}. These two levels are often being observed in our proton irradiated GaAs solar cells, as will be discussed later in this report.

3.2 Observation of Defect levels By the DLTS Technique in Proton Irradiated GaAs Solar Cells

We have conducted an extensive study of the deep-level defects in proton irradiated GaAs solar cells grown by infinite melt LPE technique over a wide range of proton energies (i.e., 50 KeV to 10 MeV) and proton fluences (10^{10} to 10^{13} P/cm^2). In general, the observed deep-level electron and hole traps depend strongly on the proton energy and proton fluence used; the defect energy level and density were found to depend on both the proton energy and proton fluence. Table 3.2 lists the defect energy levels in the proton irradiated GaAs sample observed by the DLTS technique. Note that except the 1 MeV proton irradiated GaAs samples which are the bulk GaAs materials, the rest of the samples were all LPE grown GaAs solar cells.

Table 3.2 Deep-Level Defects Observed in the Proton Irradiated GaAs Solar Cells

	Defect Levels (eV)	Proton Energy/Fluence (P/cm^2)								
		100 KeV	200 KeV			290 KeV		1 MeV*	10 MeV	
		10^{12}	10^{11}	10^{12}	10^{13}	10^{11}	10^{12}	6×10^{12}	10^{12}	10^{13}
Electron Traps	E_c-0.11	-	-	-	-	-	Δ	-	-	-
	-0.14	-	-	Δ	-	-	-	Δ	-	-
	-0.20	-	-	-	-	Δ	-	-	-	-
	-0.31	Δ	-	Δ	Δ	-	Δ	Δ	Δ	Δ
	-0.52	-	-	-	-	-	-	Δ	-	-
	-0.60	Δ	Δ	Δ	Δ	-	-	Δ	Δ	Δ
	-0.71	-	Δ	-	-	Δ	Δ	Δ	-	-
Hole Traps	E_v+0.17	Δ	-	Δ	-	Δ	-	-	-	-
	+0.29	-	-	-	-	-	-	-	Δ	-
	+0.41	-	-	-	Δ	-	Δ	-	-	-
	+0.52	-	Δ	Δ	Δ	-	-	-	Δ	Δ
	+0.57	Δ	-	-	-	-	Δ	-	-	-
	+0.71	Δ	Δ	-	Δ	Δ	-	-	-	-

*Bulk GaAs materials; others are GaAs LPE layers grown at HRL. The Measured density of these defects was found to vary between 10^{12} and 10^{14} cm^{-3} depending on the proton fluence and energy used.

The bulk GaAs samples apparently have more native defects than those of the LPE samples, and as a result the defect spectra were more complex for the bulk GaAs than the LPE samples. The dominant electron traps in these proton irradiated GaAs samples are the E_c-0.60 and E_c-0.71 eV levels which might be attributed to the GaAs antisite complex, as discussed in the preceding section while the dominant hole traps are due primarily to the E_v+0.52 and E_v+0.71 eV levels. These deep-level electron and hole traps can serve as effective recombination centers in the proton irradiated GaAs solar cells. The energy levels generated by the low energy protons are similar to those produced by the one-MeV electron irradiation as being reported in the literature [3].

IV. RESULTS AND DISCUSSION

The major technical findings made in this research program will be discussed in this chapter. We shall first present a brief summary of our previous study on the forward I-V and DLTS measurements on samples irradiated with different proton energies and proton fluences. We then focus our discussion on the periodic thermal annealing behavior of the 200 KeV proton irradiated samples. Calculations of the damage constants for the 200 KeV proton irradiated GaAs solar cells are made based on the hole diffusion length data deduced from the SEM-EBIC data and DLTS results.

4.1 I-V and DLTS Characteristics vs. Proton Energy and Fluence, and the Effect of 300° C Thermal Annealing

The open circuit voltage, V_{oc}, of a p-n junction solar cell depends strongly on the value of dark currents which consist mainly of recombination and diffusion current components [2]. In the radiation damaged cells, the recombination current in the junction space charge region of the cell plays a dominant role in controlling the dark current of the solar cell; this is usually the case for the GaAs solar cells. Thus, it is important to study the forward I-V characteristics of the proton irradiated GaAs solar cells under dark conditions to determine the dominant current

component in the cells. From such a study, it is often possible to deduce the effective lifetimes in the junction space charge region of the cell and to correlate the results with the deep-level defects determined by the DLTS measurements. We shall discuss the results of our I-V measurements next. Fig. 4.1 shows the I-V characteristics curves under forward bias conditions as functions of proton energy and fluence with E_p = 200, 800 KeV, and 10 MeV, and $\phi_p = 10^{11}$, 10^{12}, and 10^{13} P/cm^2. The results showed that the unirradiated sample has the lowest dark current, followed by 800 KeV irradiated samples with proton fluence of 10^{12} P/cm^2 and 200 KeV irradiated samples with $\phi_p = 10^{11}$ P/cm^2. The unannealed 200 KeV proton irradiated samples with $\phi_p = 10^{13}$ P/cm^2 has the highest dark current, followed by the 10 and 0.8 MeV samples irradiated by the same proton fluence. A 300 °C thermal annealing for one hour greatly reduces the dark current of the 200 KeV irradiated samples. The reason for the decrease in the dark current of the 200 KeV proton irradiated samples followed by a 300 °C thermal annealing process can be attributed to the reduction of the defect density in the junction space charge region of these cells, as can be shown by the DLTS data. Fig. 4.2 and 4.3 showed the DLTS thermal scans of electron and hole traps in the 200 KeV proton irradiated samples with proton fluence of 5×10^{11} P/cm^2, for the unannealed and 300° C annealed samples. It is clearly shown that followed a 300 °C thermal annealing for one hour the densities of electron and hole traps are reduced significantly. Note that a good correlation exists between the observed dark current shown in Fig. 4.1 and the defect densities deduced from Fig. 4.2 and Fig. 4.3. Table 4.1 lists the measured defect parameters in the 200 KeV proton irradiated GaAs cells before and after 300 °C thermal annealing. Calculations of the effective lifetimes in the junction space charge region of the 100 and 200 KeV proton irradiated GaAs solar cells from the forward I-V characteristics curves are illustrated in Fig. 4.4, which showed the effective lifetimes varying

from 4ns for the unirradiated sample to 0.025 and 0.07 ns for the 100 and 200 KeV irradiated samples with $\phi_p = 10^{13}$ P/cm^2. It was found that a 300 °C thermal annealing for one hour can restore the effective carrier lifetimes by a factor of two to three. Thus low temperature thermal annealing is clearly beneficial in that it reduces the defect density and the dark current and recovers the lifetimes and power loss due to radiation damage. The result of this initial annealing study on the 200 KeV proton irradiated GaAs solar cells has led us to the final phase of study on the effects of periodic thermal annealing on the deep-level defects and the performance of 200 KeV proton irradiated GaAs solar cells. The results will be discussed in sections 4.2 and 4.4.

Fig. 4.5 and Fig. 4.6 showed the DLTS thermal scans of electron and hole traps respectively, for four different proton energies and proton fluence of 10^{12} P/cm^2. The results showed that both 200 and 290 KeV proton irradiated samples have two to three electron and hole trap levels, and the density of each defect level observed was higher than that of 100 KeV and 10 MeV proton irradiated samples. Among samples studied, the 10 MeV proton irradiated samples showed the least damage. This is due to the fact that 10 MeV protons penetrate much deeper into the cell (> 10μm) than the low energy proton irradiated cells, and most of the damages were done outside the active region of the cell. On the contrary, in the 200 KeV and 290 KeV proton irradiated samples the penetration depths are within 1 to 2 μm from the junction and the damage falls in the active region of the n-GaAs LPE layer. Thus, damages produced by these low energy protons are far more extensive than other proton energies used in this study; this is clearly shown in Fig. 4.5 and Fig. 4.6. Fig. 4.7 and Fig. 4.8 are the DLTS thermal scans of electron and hole traps for the 10^{13} P/cm^2 proton fluence and for three different proton energies. The results again showed that defect density and defect energy levels are higher and more complex for the 200 KeV and 290 KeV irradiated

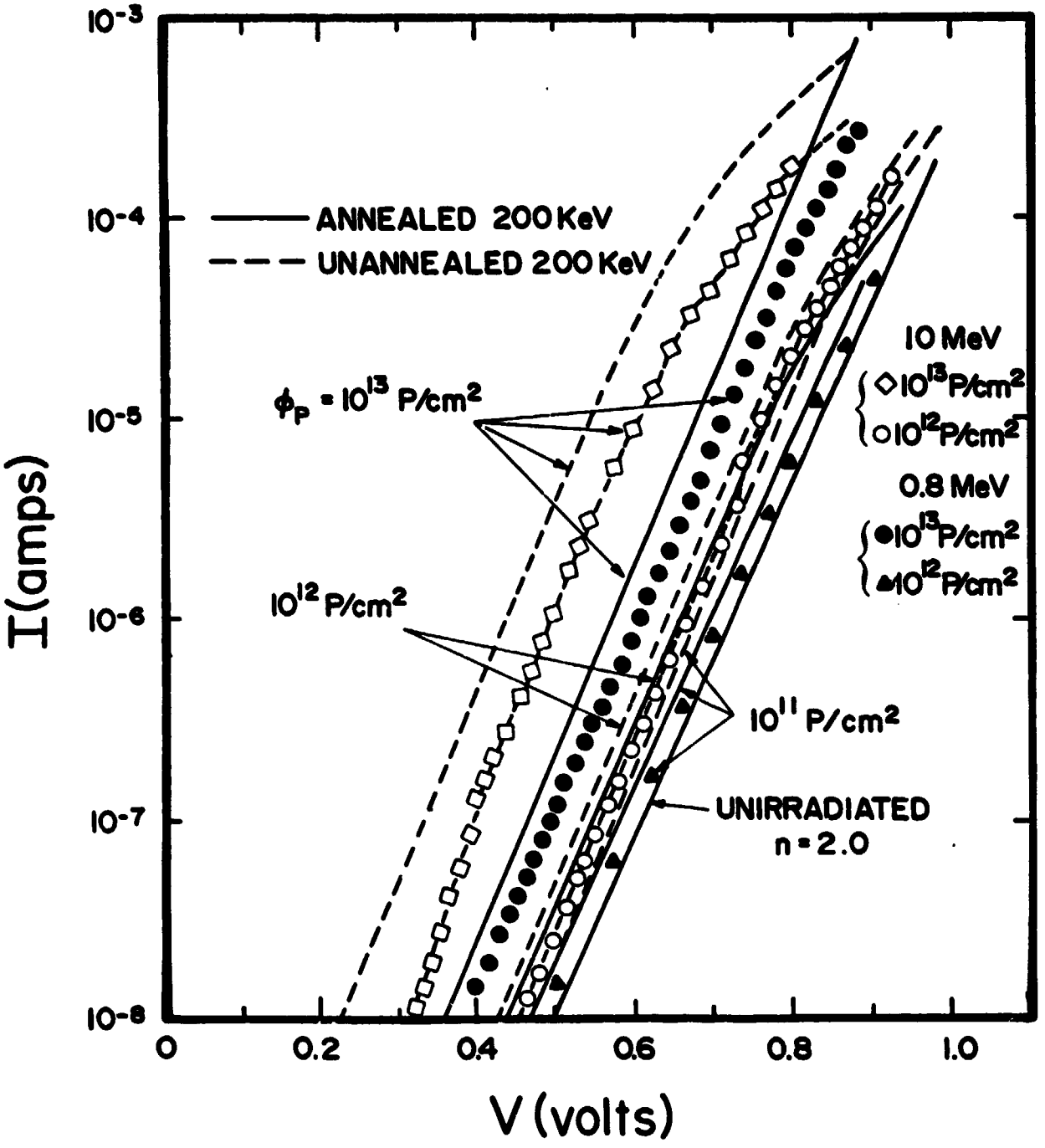

Fig. 4.1 Forward I-V characteristics vs. proton energies and proton fluence in proton irradiated GaAs mesa diodes.

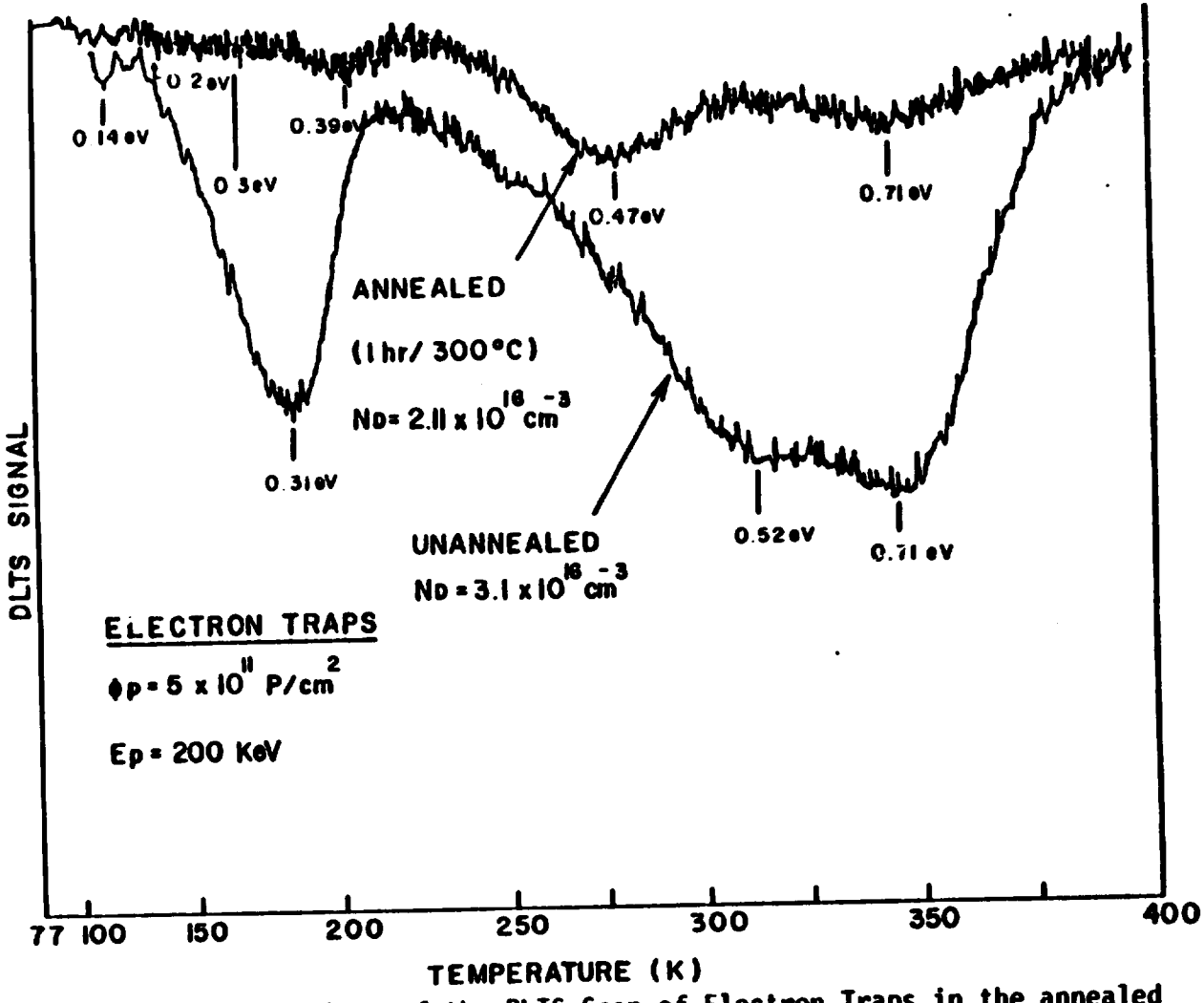

Fig. 4.2 A comparison of the DLTS Scan of Electron Traps in the annealed and unannealed 200 KeV proton irradiated sample

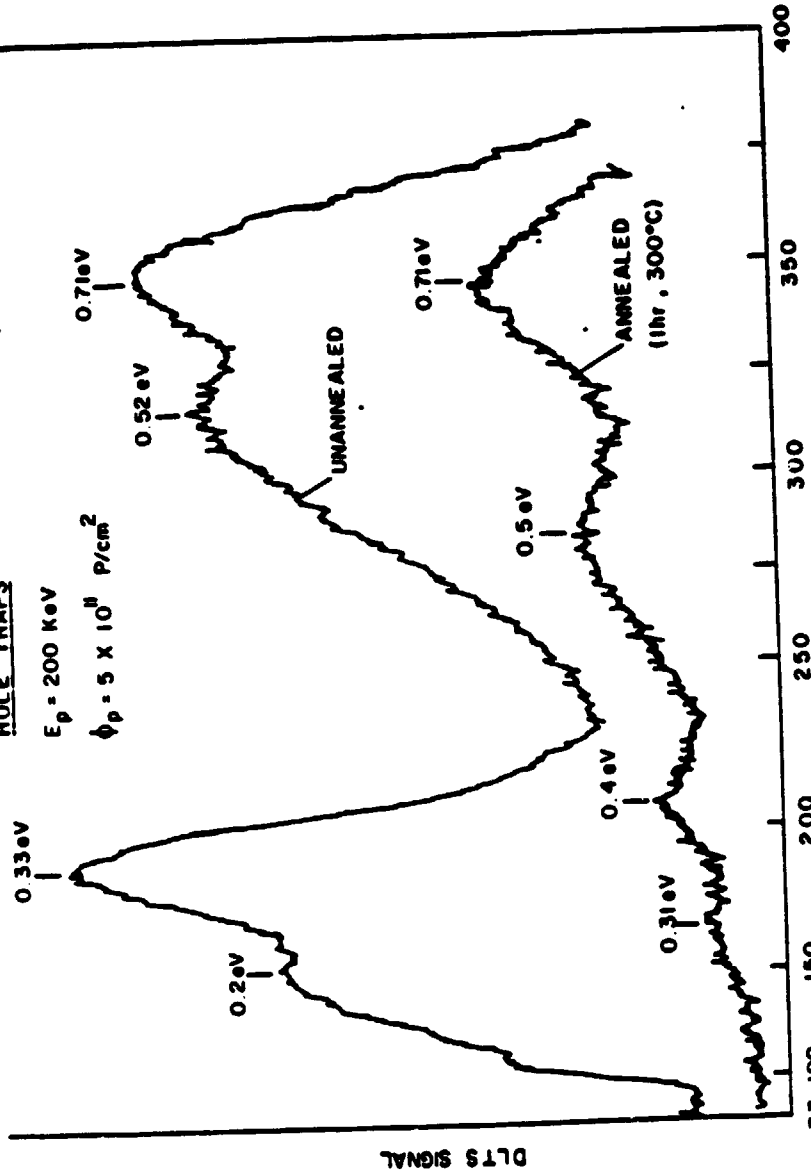

Fig. 4.3 A comparison of DLTS scan of Hole Traps for the annealed and unannealed AlGaAs-GaAs Sample

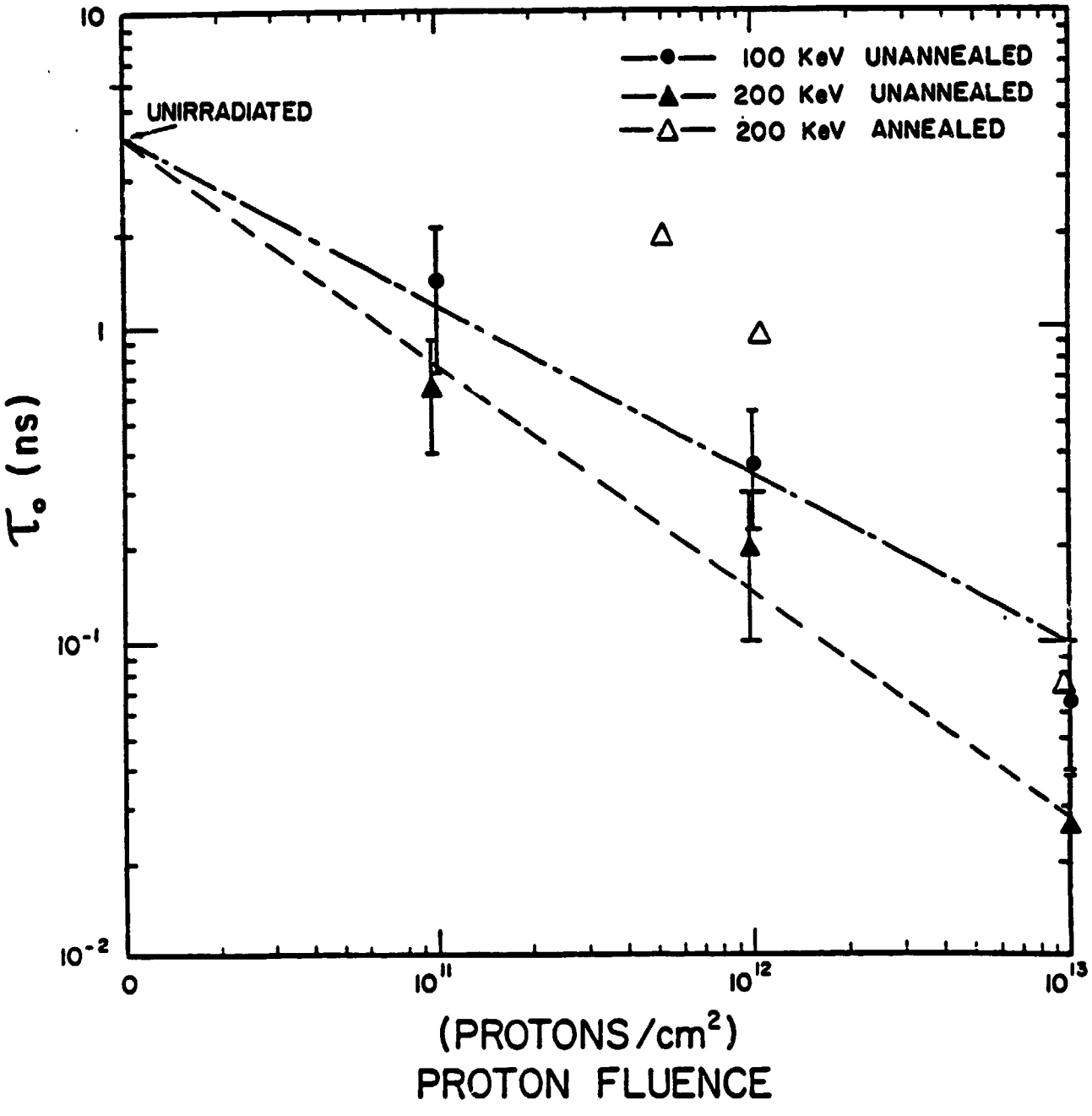

Fig. 4.4 Effective Lifetimes vs. Proton Fluence in the 100 and 200 KeV proton irradiated AlGaAs-GaAs diodes

Table 4.1 Measured Defect Parameters in 200 KeV Proton Irradiated AlGaAs-GaAs Solar Cells Before and After 300° C Thermal Annealing

Proton Fluence	A or U	Electron traps				Hole traps			
		origin of defect	level (eV)	density (cm^{-3})	capture cross section (cm^{-2})	origin of defect	level (eV)	density (cm^{-3})	capture cross section (cm^{2})
$5x10^{11}$	U	AsGa	0.14	$3.23x10^{-2}$	$1.59x10^{-16}$	-	0.2	$6.58x10^{13}$	
		V_{Ga}	0.31	$5.2\ x10^{13}$	$1.79x10^{-14}$	-	0.33	$9.68x10^{13}$	$9.73x10^{-15}$
		$V_{Ga}V_{As}$	0.52	$5.9\ x10^{13}$	$4.93x10^{-14}$	Fe	0.52	$6.85x10^{13}$	$6.64x10^{-14}$
		"B"	0.71	$4.84x10^{13}$	$4.79x10^{-14}$	"B"	0.71	$7.88x10^{13}$	$4.16x10^{-13}$
	A	AsGa	0.2	$5.2\ x10^{11}$	$1.04x10^{-16}$				
		V_{Ga}	0.3	$2.1\ x10^{12}$	$2.4\ x10^{-14}$	-	0.31	$5.14x10^{12}$	
		-	0.39	$1.24x10^{12}$	$5.5\ x10^{-14}$	"A"	0.4	$1.24x10^{13}$	$1.02x10^{-16}$
		-	0.47	$1.06x10^{13}$	$4.03x10^{-15}$	Fe	0.5	$1.7\ x10^{13}$	$6.74x10^{-14}$
		"B"	0.71	$1.21x10^{13}$	$4.86x10^{-14}$	"B"	0.71	$2.91x10^{13}$	$5.3\ x10^{-13}$
$1x10^{12}$	U	AsGa	0.14	$8.45x10^{12}$	$2.9\ x10^{-16}$	-	0.2	$1.61x10^{14}$	
		V_{Ga}	0.31	$7.15x10^{13}$	$2.2\ x10^{-14}$	-	0.33	$2.06x10^{14}$	$5.4\ x10^{-15}$
		$V_{Ga}V_{As}$	0.52	$6.93x10^{13}$	$5.5\ x10^{-15}$	Fe	0.52	$9.6\ x10^{13}$	$1.28x10^{-13}$
		-	0.71	$6.83x10^{13}$	$5.05x10^{-14}$	"B"	0.71	$9.83x10^{13}$	
	A	AsGa	0.2	$1.2\ x10^{12}$	$8.91x10^{-16}$	-	0.19	$7.7\ x10^{12}$	
		V_{Ga}	0.3	$4.78x10^{12}$	$2.26x10^{-14}$	-	0.31	$1.16x10^{13}$	$1.0\ x10^{-15}$
		-	0.39	$5.8\ x10^{12}$	$6.4\ x10^{-14}$	"A"	0.4	$1.34x10^{13}$	$6.1\ x10^{-15}$
		-	0.47	$1.9\ x10^{13}$	$2.81x10^{-15}$	Fe	0.5	$3.68x10^{13}$	$1.1\ x10^{-13}$
		"B"	0.71	$1.4\ x10^{13}$	$5.1\ x10^{-14}$	"B"	0.71	$1.35x10^{13}$	$4.0\ x10^{-13}$
$1x10^{13}$	U	AsGa	0.14	$2.8\ x10^{13}$	$1.71x10^{-16}$	-	0.2	$2.25x10^{14}$	
		V_{Ga}	0.31	$2\ \ x10^{13}$	$2.39x10^{-14}$	-	0.33	$3.7\ x10^{14}$	$6.0\ x10^{-15}$
		$V_{Ga}V_{As}$	0.52	$1.99x10^{14}$	$5.42x10^{-15}$	Fe	0.52	$3.47x10^{14}$	$1.29x10^{-13}$
		"B"	0.71	$7.1\ x10^{13}$	$4.92x10^{-14}$				
	A	AsGa	0.2	$2.97x10^{12}$	$9.62x10^{-16}$	-	0.19	$7.3\ x10^{13}$	
		V_{Ga}	0.3	$6.48x10^{12}$	$1.93x10^{-14}$	-	0.31	$5.0\ x10^{13}$	
		-	0.39	$1.96x10^{13}$	$7.26x10^{-14}$	"A"	0.4	$1.1\ x10^{14}$	$5.9\ x10^{-15}$
		-	0.51	$6.18x10^{13}$	$5.37x10^{-15}$	Fe	0.51	$1.92x10^{14}$	$1.2\ x10^{-13}$
		"B"	0.71	$5.74x10^{13}$	$4.86x10^{-16}$	"B"	0.76	$4.8\ x10^{13}$	

Fig. 4.5 DLTS scans of electron traps vs. proton energy, with $\phi_p = 10^{12}$ P/cm^2.

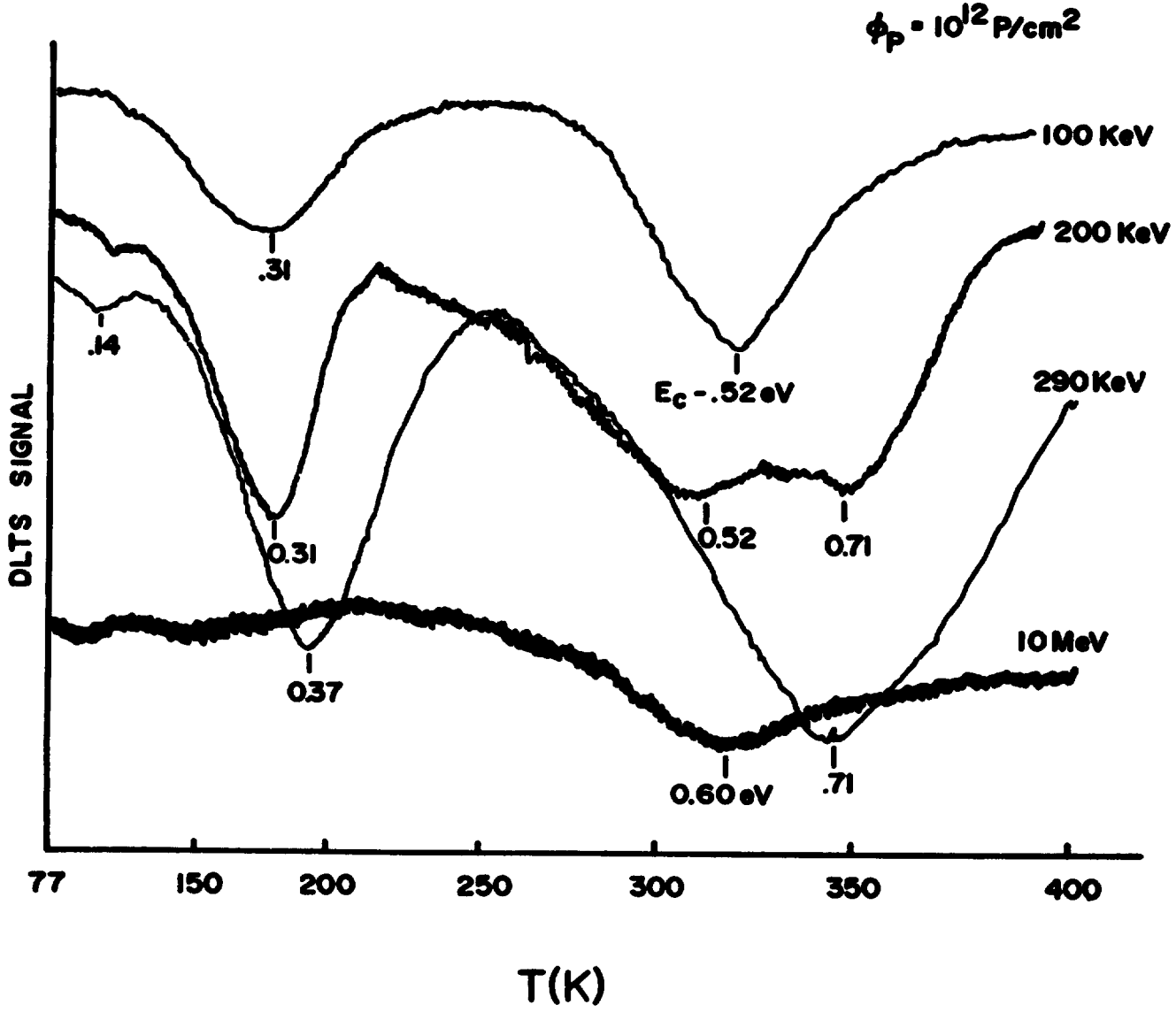

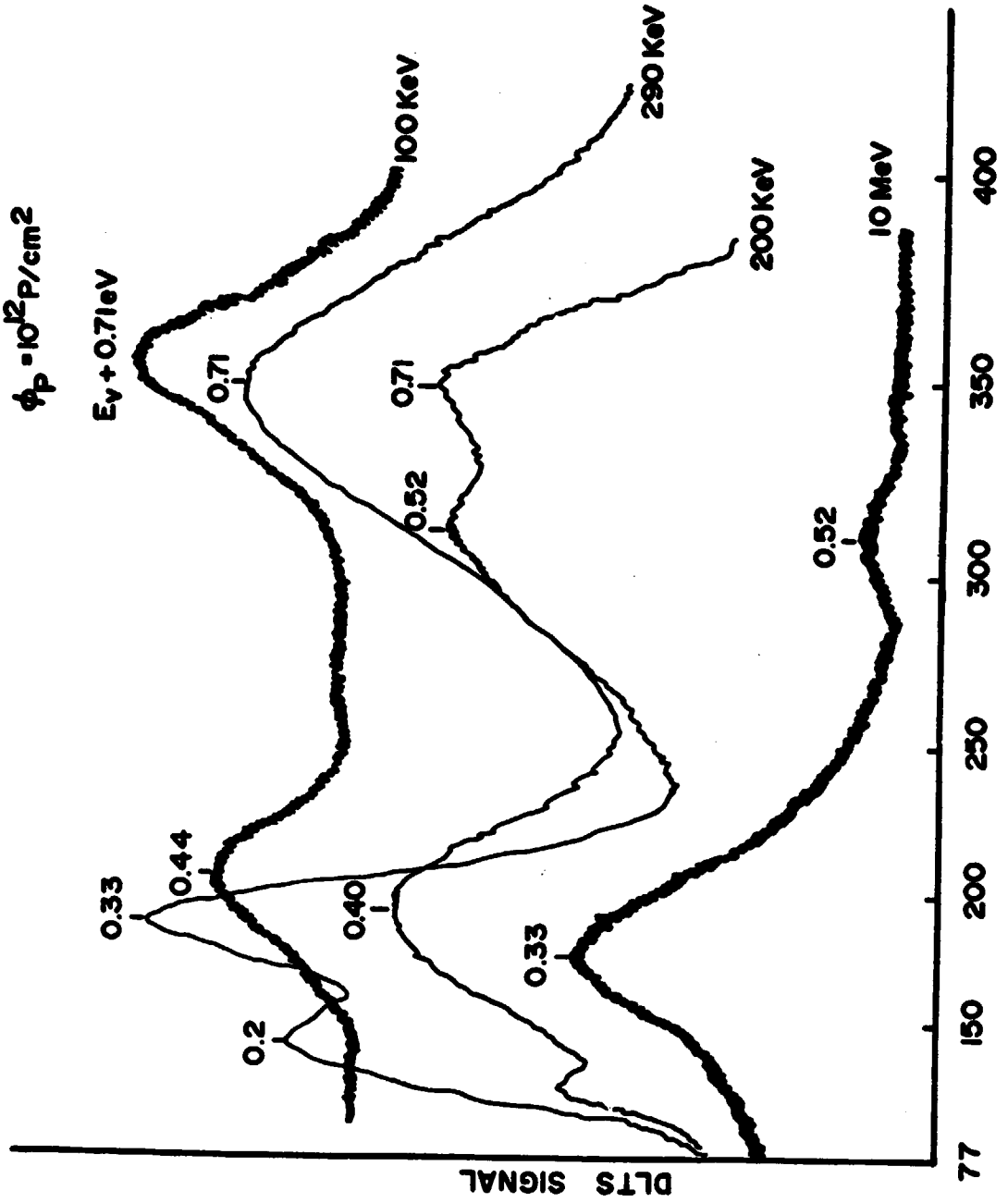

Fig. 4.6 DLTS scans of hole traps vs. proton energy, with $\phi_p = 10^{12}$ P/cm^2.

Fig. 4.7 DLTS scans of electron traps vs. proton energy, with $\phi_p + 10^{13}$ P/cm^2.

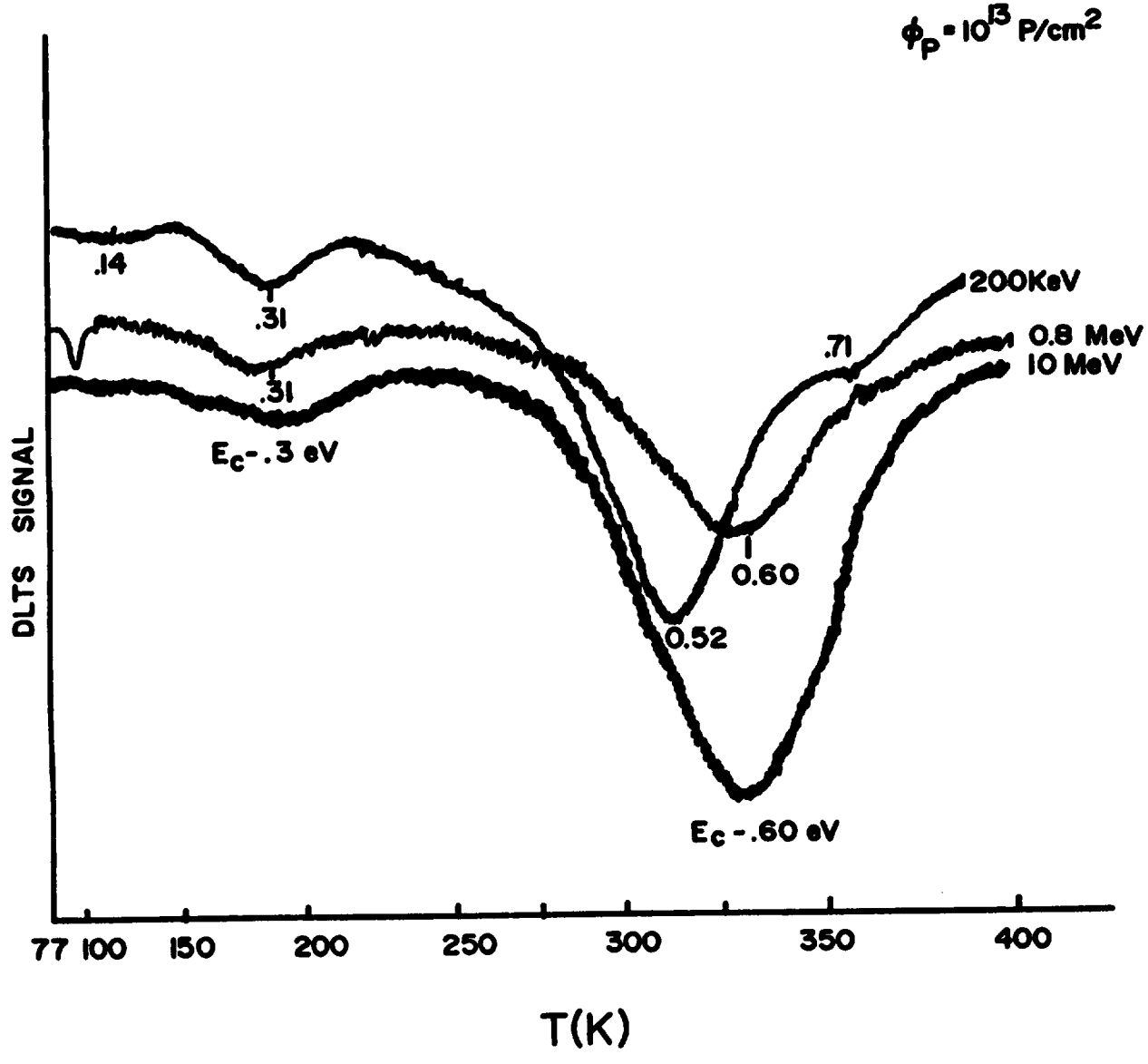

Fig. 4.8 DLTS scans of hole traps vs. proton energy, with $\phi_p = 10^{13}$ P/cm^2.

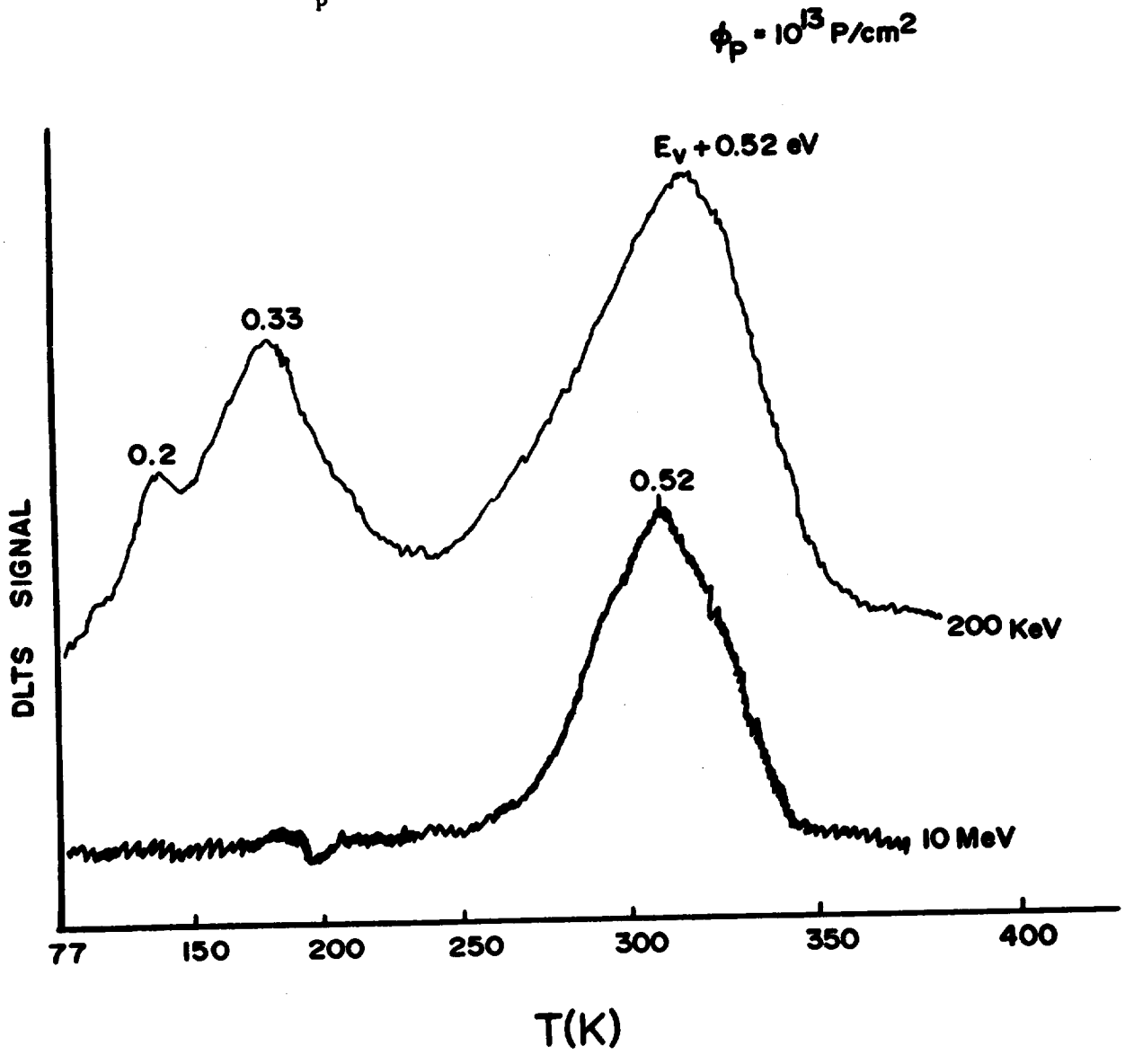

samples than the others.

Based on the results of Fig. 4.5 through Fig. 4.8 and with the solar cell structure shown in Fig. 2.1, it is concluded that the 200 KeV proton irradiation should represent the worst case proton damage. Thus, we have focussed our present research efforts on study of the influence of low temperature periodic thermal annealing process on the proton induced deep-level defects and the performance of GaAs solar cells. The results of this study are discussed next.

4.2 Periodic Thermal Annealing study in the 200 KeV Proton Irradiated GaAs solar cells

In the study of the influence of the periodic thermal annealing process on the deep-level defects in the 200 KeV proton irradiated GaAs solar cells, we have chosen the initial proton fluence of 10^{11} P/cm^2 which corresponds to the highest value for all protons capable of traversing a 12 mil coverglass during 11 years in geosynchronous orbit and represent the worst possible case. Three annealing temperatures of 200, 300, and 400 °C were used in this study. The samples were annealed at 200 °C for 24 hours, 300 °C and 400 °C for 6 hours, respectively. The I-V, C-V, and DLTS experiments were then performed on each of these annealed samples, and the results were compared with the unannealed samples. The same proton irradiation and thermal annealing processes were performed on the 200 KeV irradiated samples up to four cycles. Thus, for the fourth irradiation cycle, the cumulative proton fluence is 4×10^{11} P/cm^2, and the samples were annealed four times at 200, 300, and 400 °C, respectively. The results of our I-V, C-V, and DLTS measurements are shown in Fig. 4.9 through Fig. 4.31. Fig. 4.9 through Fig. 4.12 showed the forward I-V characteristics curves for the first, second, third, and fourth irradiation and annealing cycles, respectively; the proton fluences are given respectively by 10^{11}, 2×10^{11}, 3×10^{11}, and 4×10^{11} p/cm^2 in each cycle. Fig. 4.9 shows the forward I-V curves for the first irradiation and annealing cycle with $\Phi_p = 10^{11}$ P/cm^2 and annealed temperatures at 200, 300, and 400° C, respectively. The results showed that the unannealed

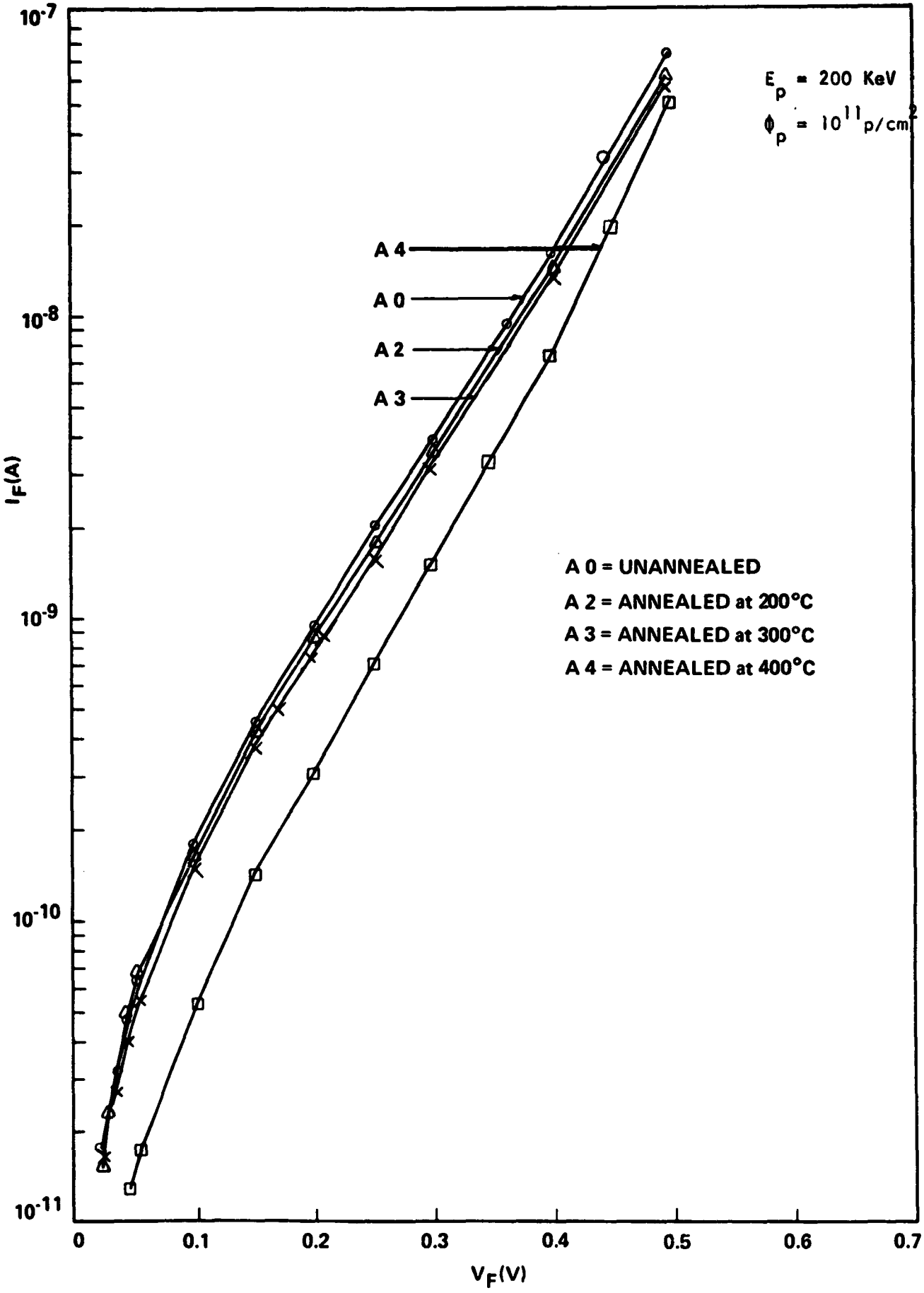

Fig. 4.9 Forward I-V characterics curves for the 200 KeV proton irradiated samples, with ϕ_p = 10^{11} P/cm^2 and T_A = 0, 200, 300, 400 °C.

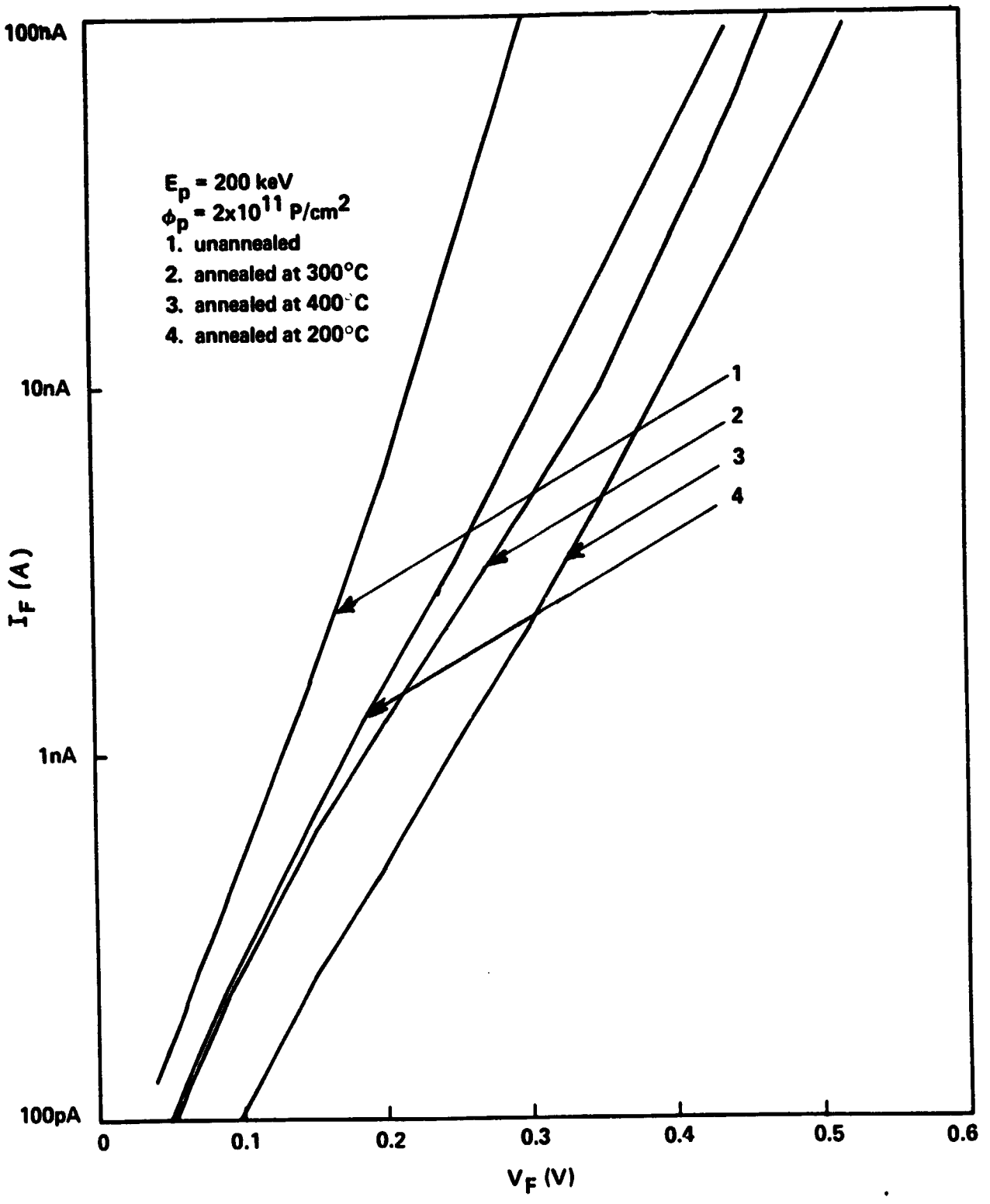

Fig. 4.10 Forward I-V characteristics curves for the 200 KeV proton irradiated samples with ϕ_p = 2x10^{11} P/cm^2 and T_A = 0, 200, 300, and 400° C.

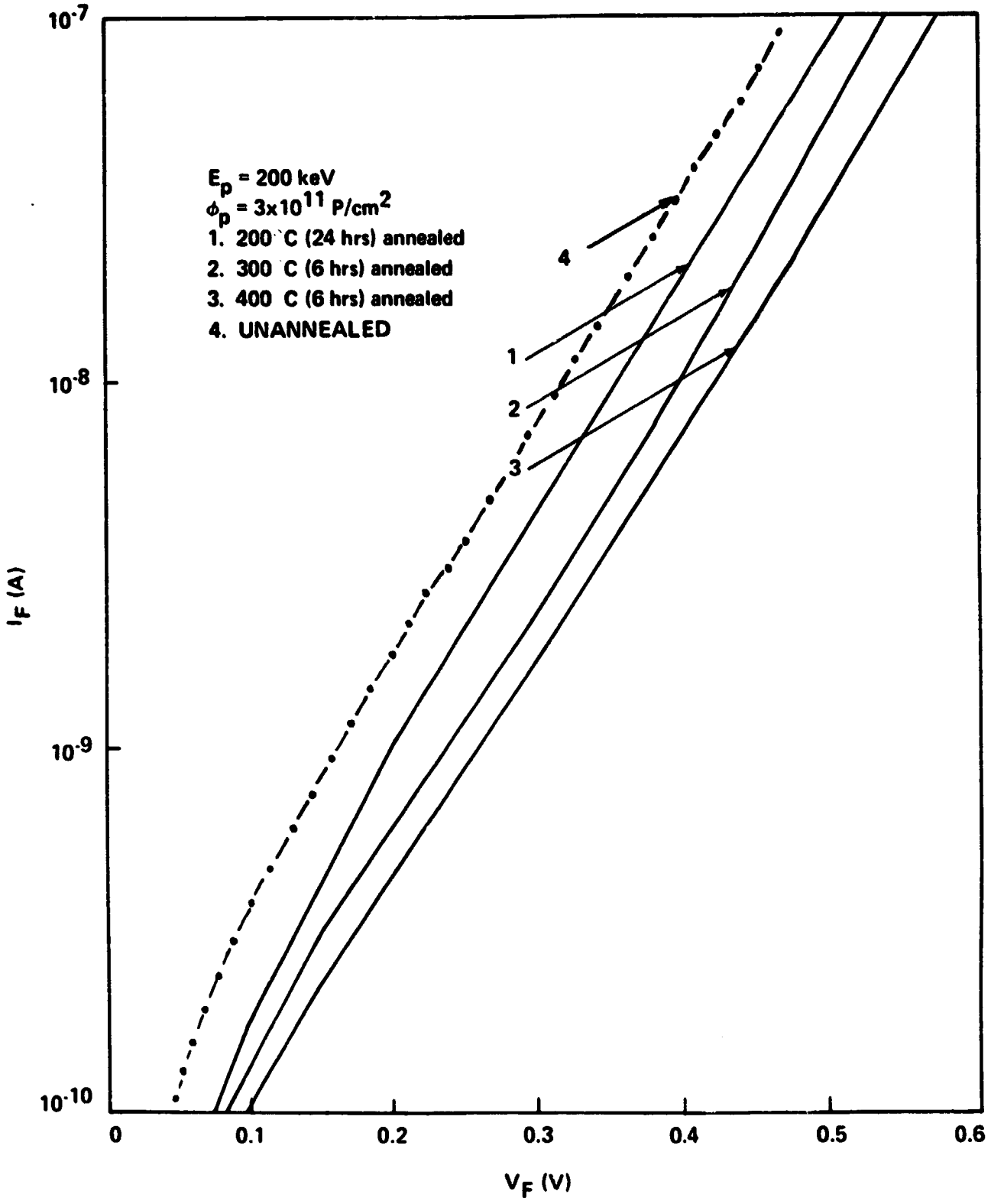

Fig. 4.11 Forward I-V characteristic curves for the 200 KeV proton irradiated sample with ϕ_p = 3x10^{11} P/cm^2 and T_A = 0, 200, 300, and 400° C.

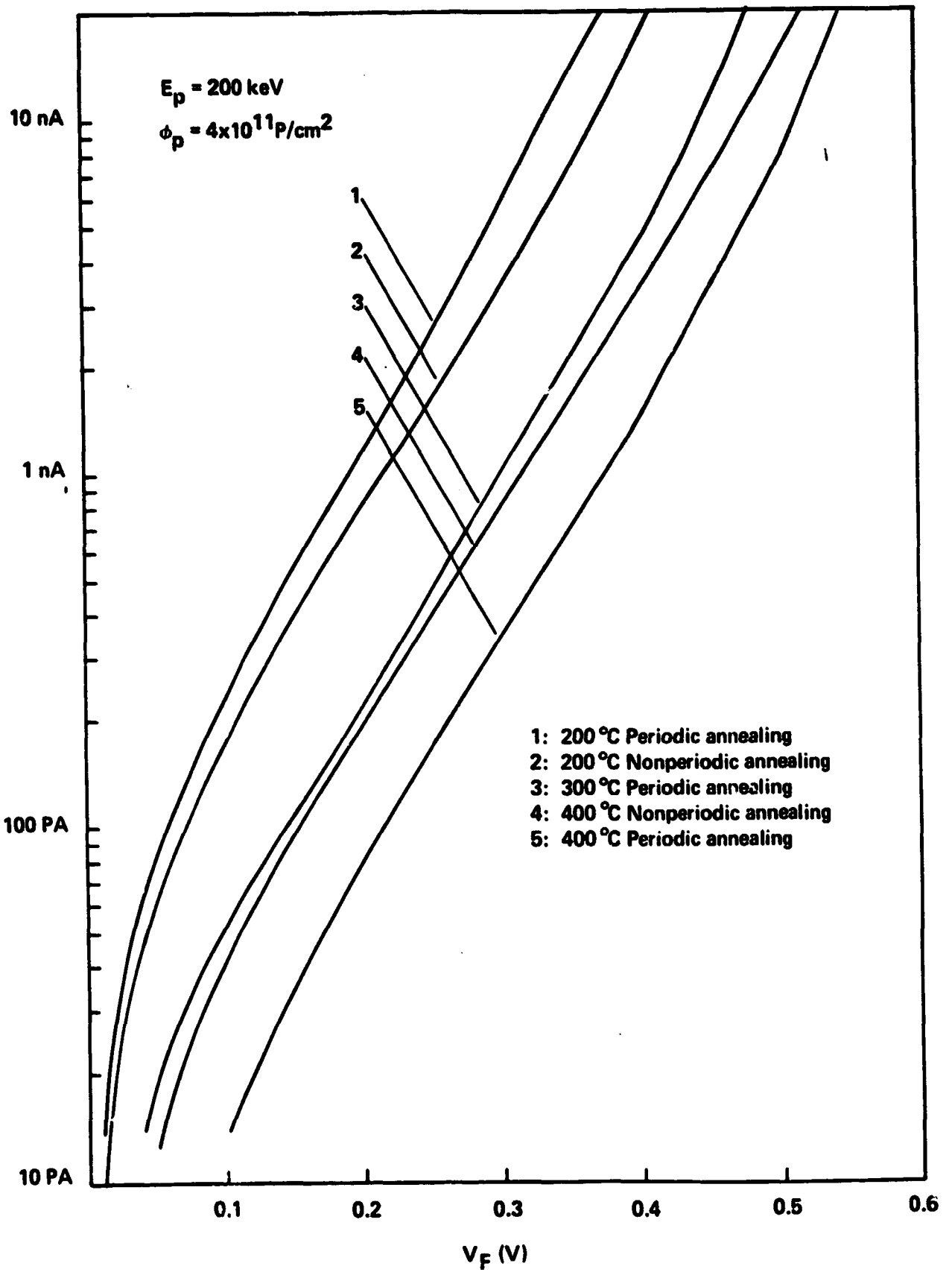

Fig. 4.12 Forward I-V characteristic curves for the 200 KeV proton irradiated samples with ϕ_p = 4x10^{11} P/cm^2, and T_A = 200, 300, and 400° C.

sample has the highest dark current, followed by 200, 300, and 400 °C annealed samples. Thus, it is obvious that the effect of thermal annealing is to reduce the dark recombination current in the proton irradiated GaAs solar cells; increasing annealing temperature would further reduce the dark current. This same trend was observed in all the irradiation and annealing cycles shown in Fig. 4.9 to Fig. 4.12. The decrease in the dark recombination current with increasing annealing temperature can be attributed to the reduction of defect density in the junction space charge region with increasing annealing temperature as will be shown later in the DLTS data. The reverse I-V characteristics for the 200 KeV proton irradiated samples with four different irradiation and annealing cycles are shown in Fig. 13 through Fig. 16. The results are consistent with the forward I-V characteristics discussed above. Again, we see that the unannealed sample has the highest reverse dark current while sample annealed at 400 °C yields the lowest reverse leakage current. For the same annealing temperature, the periodic annealed samples appeared to have a slightly lower reverse dark current than the non-periodic annealed samples. Fig. 4.17 through Fig. 4.19 showed the C-V data for the first, second, and third cycle proton irradiated and annealed samples. The results showed that the capacitance variation in these samples was less than 10%, indicating that the background dopant density in these n-GaAs LPE layers was relatively constant ($\sim$ 3 to 4x10^{16} cm^{-3}), independent of the annealing temperature or proton fluence. This is an indicative of little or no carrier removal occured as a result of the proton irradiation. We shall next discuss the results of our DLTS measurements on these periodically annealed and irradiated samples.

As discussed above, the decrease in the dark forward and reverse currents in the 200 KeV proton irradiated samples with increasing annealing temperature can be attributed to the reduction of defect densities in the junction space charge region of the cells with increasing annealing temperature; this can be verified by the DLTS

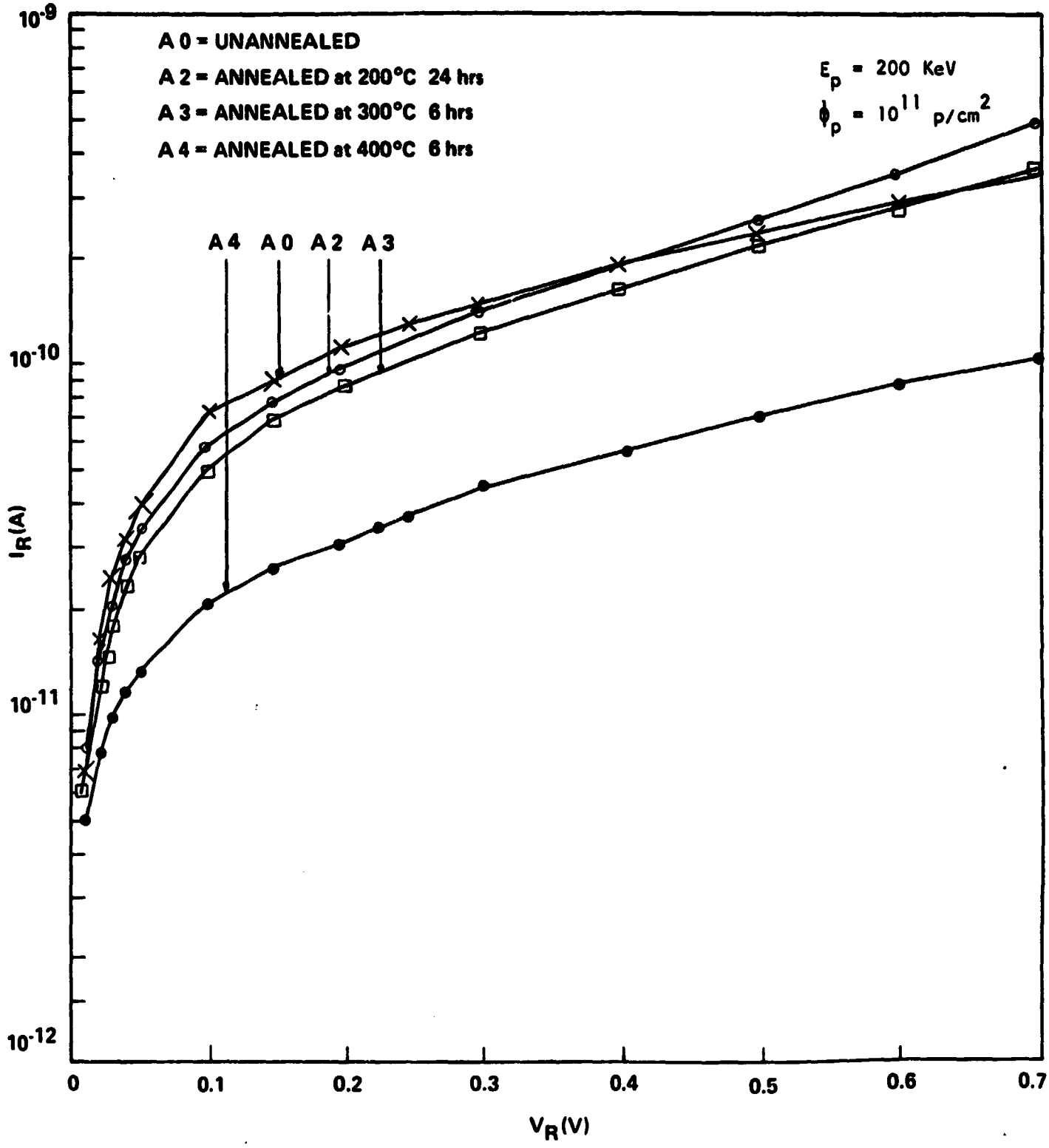

Fig. 4.13 Reverse I-V characteristic vs. annealing temperature for E_p = 200 KeV, ϕ_p = 10^{11} P/cm^2.

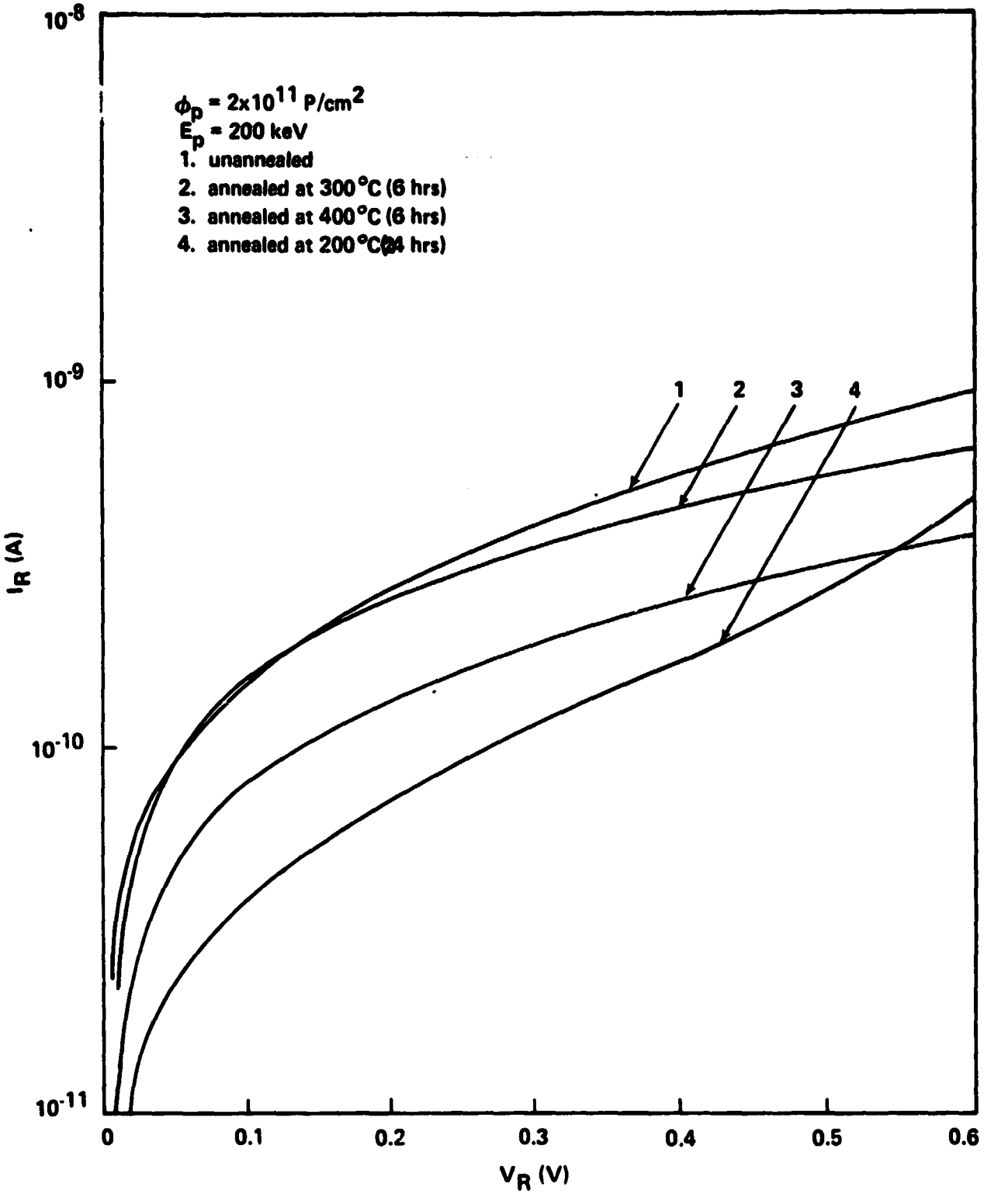

Fig. 4.14 Reverse I-V characteristic vs. annealing temperature for E_p = 200 KeV, $\phi_p = 2x10^{11}$ P/cm^2.

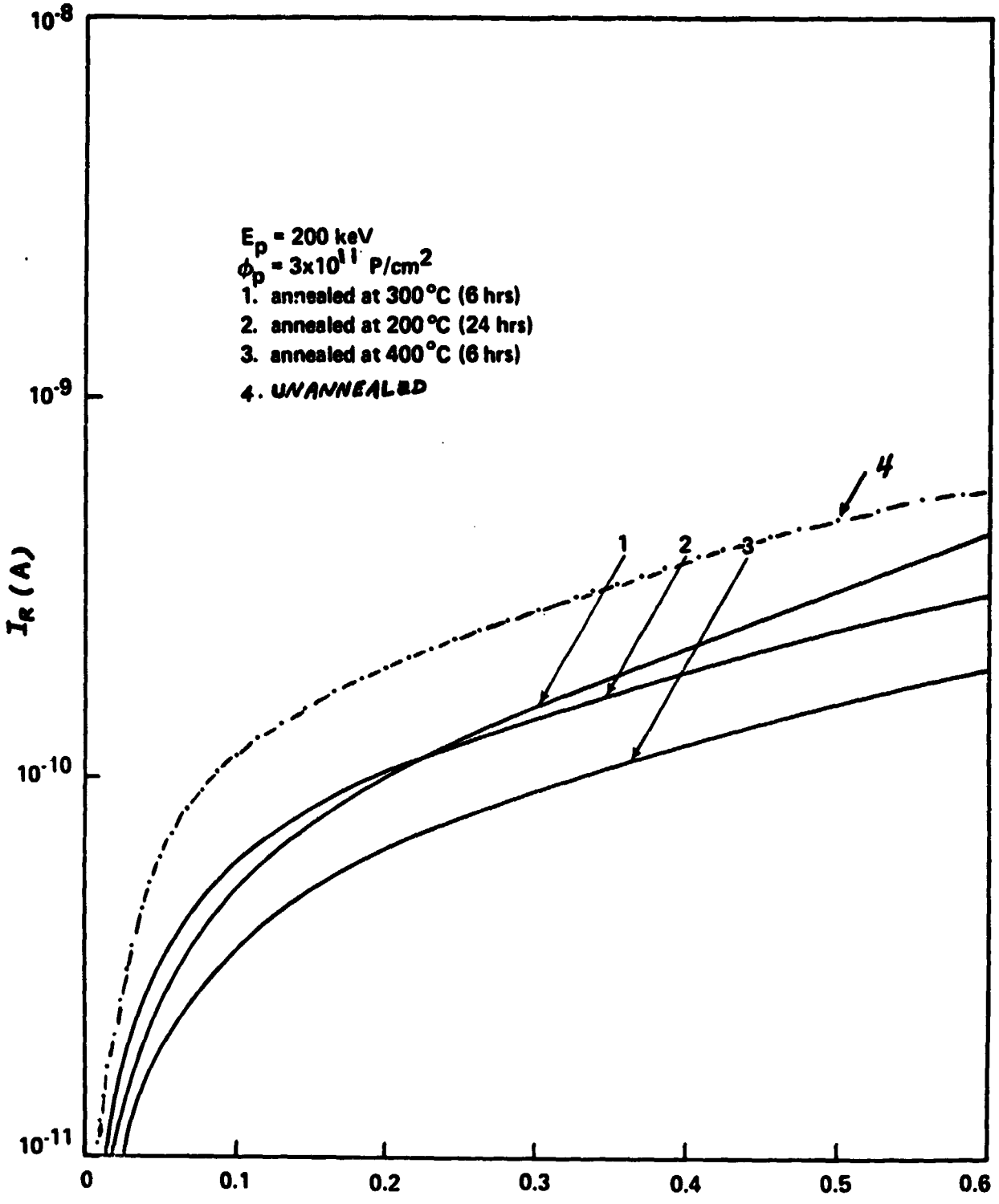

Fig. 4.15 Reverse I-V characteristic vs. annealing temperature for E_p = 200 KeV, ϕ_p = 3x10^{11} P/cm^2.

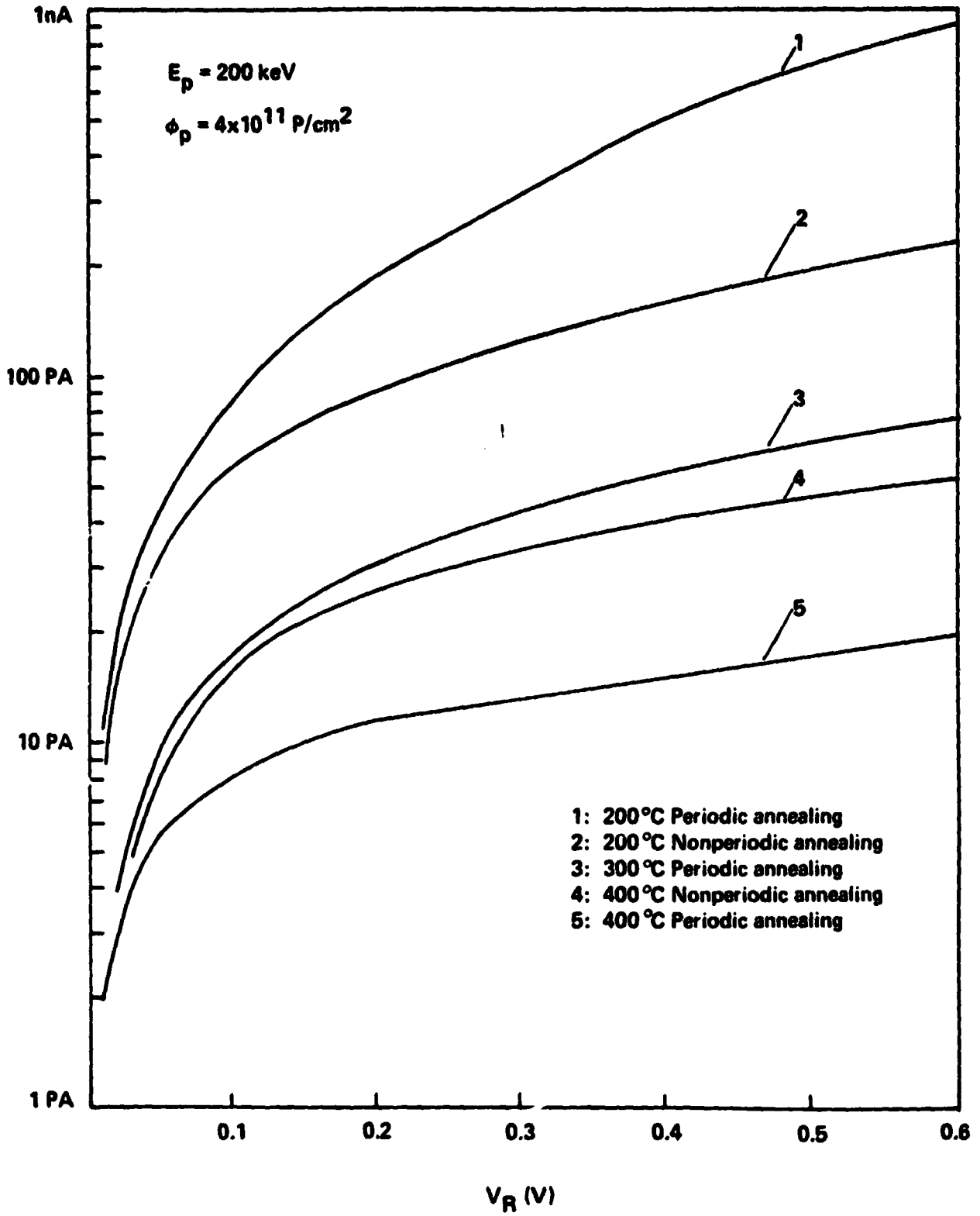

Fig. 4.16 Reverse I-V characteristic vs. annealing temperature for E_p = 200 KeV, ϕ_p = 4x10^{11} P/cm^2.

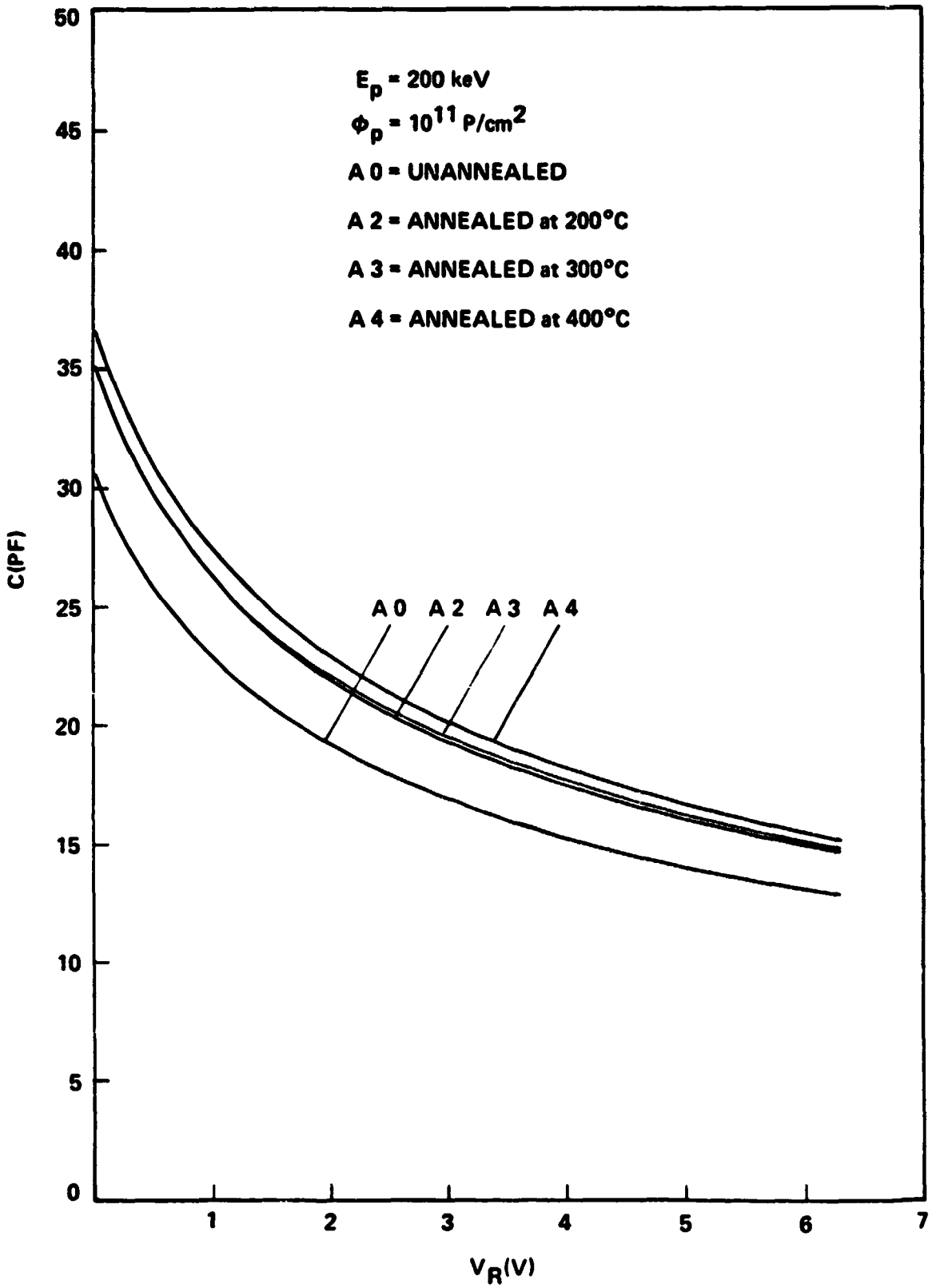

Fig. 4.17 C-V characteristic vs. annealing temperature for E_p = 200 KeV, ϕ_p = 1x10^{11} P/cm^2.

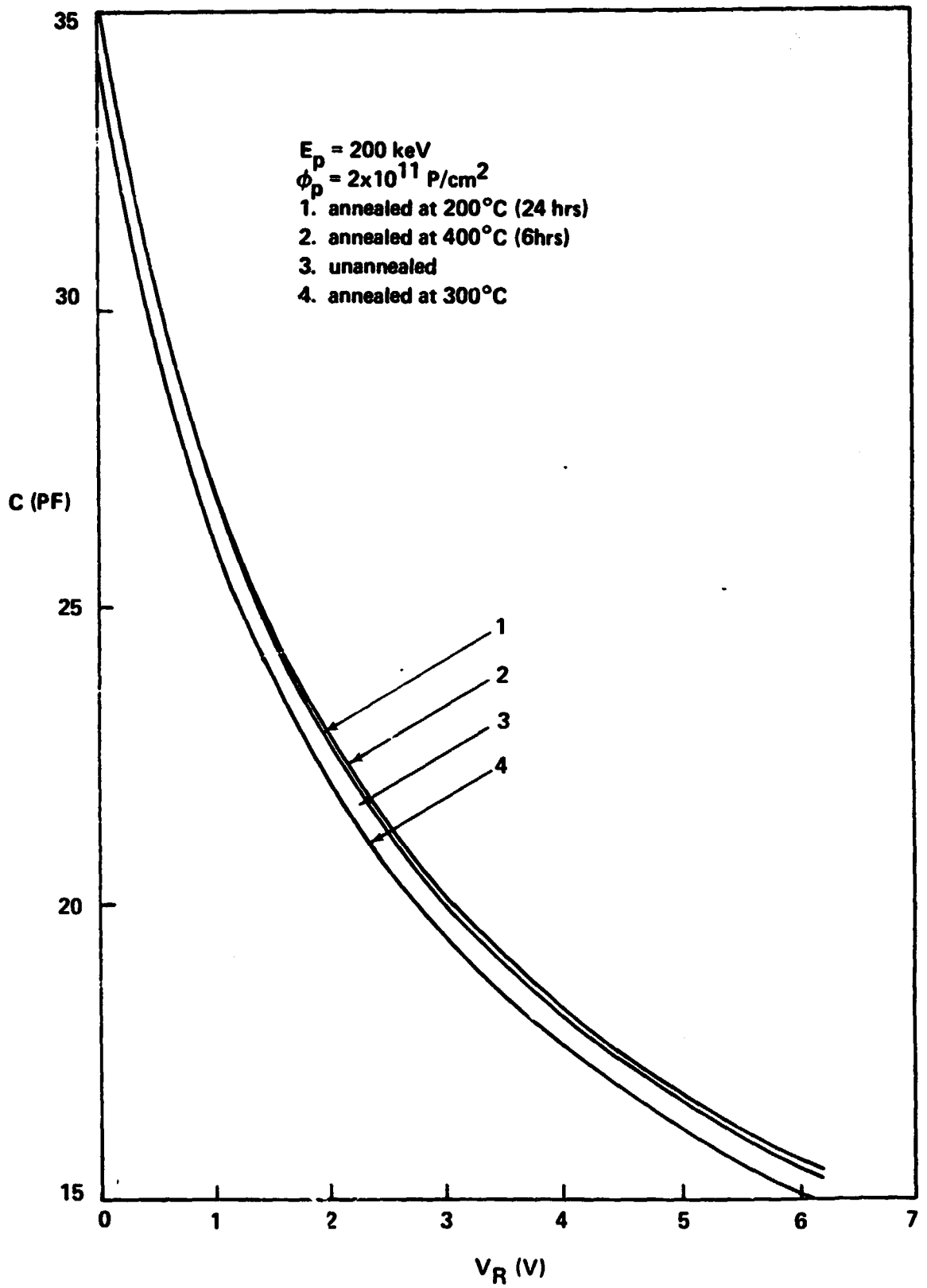

Fig. 4.18 C-V characteristic vs. annealing temperature for E_p = 200 KeV, ϕ_p = 2x10^{11} P/cm^2.

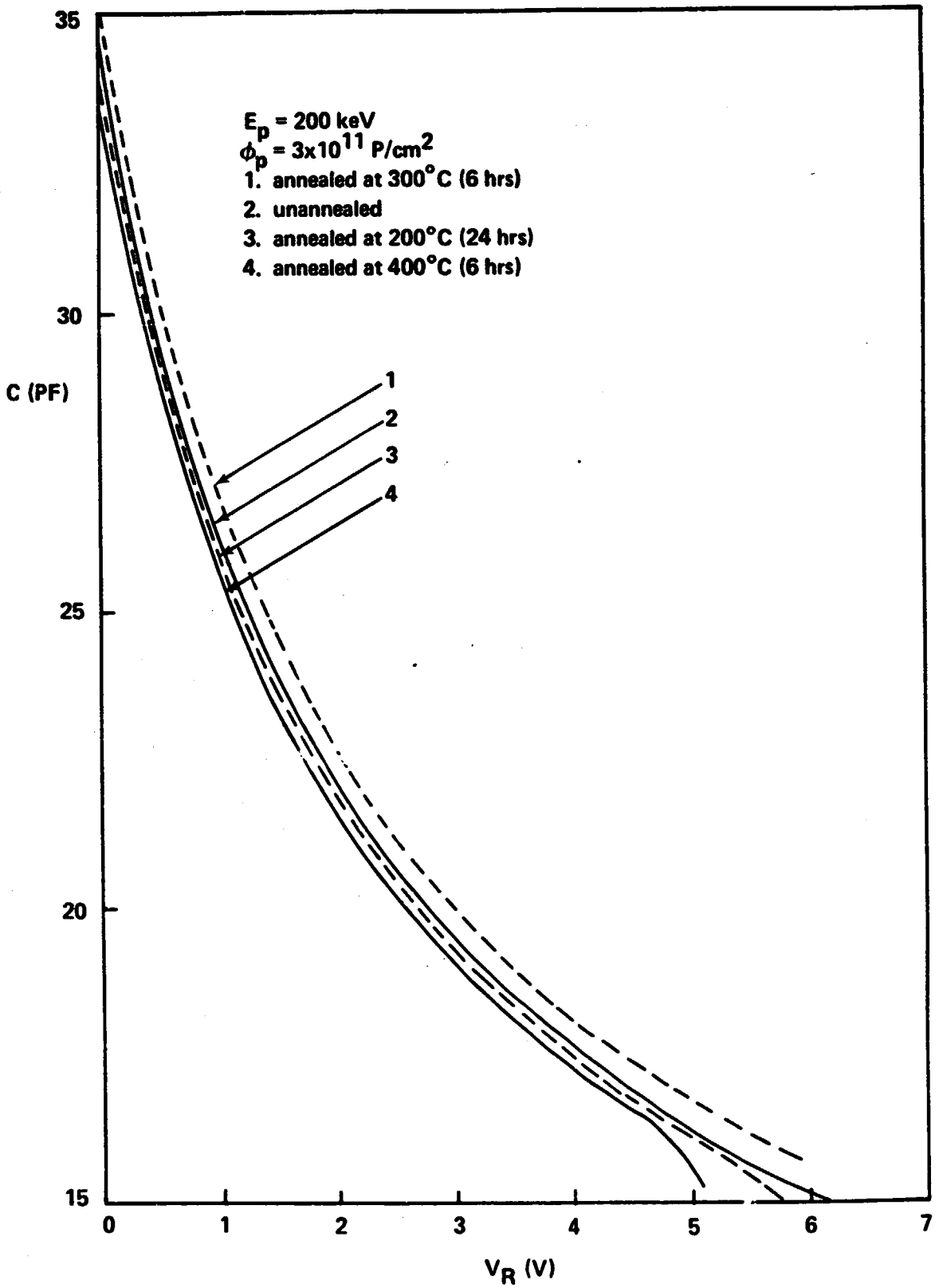

4.19 C-V characteristic vs. annealing temperature for E_p = 200 KeV, ϕ_p = 3x10^{11} P/cm^2.

data. Fig. 20 through Fig. 27 showed the DLTS thermal scans of electron and hole traps observed in the 200 KeV proton irradiated samples, periodically irradiated and annealed samples as well as unannealed samples. The main electron trap level observed was E_c-0.71 eV and the main hole trap level was E_v+0.18 eV. In addition, shallower electron trap such as E_c-0.52 eV was also observed in the unannealed samples with proton fluence of $4x10^{11}$ P/cm^2 (i.e., fourth cycle samples). Increasing annealing temperature would first anneal out the shallower traps and reduce the density of deeper trap level, E_c-0.71 eV. The results of these DLTS data clearly showed that the density of both electron and hole traps can be effectively reduced followed by a 200, 300, and 400° C thermal annealing process. Fig. 4.28 showed the density of electron trap (E_c-0.71 eV) and hole trap (E_v+0.18 eV) vs. annealing temperature for the first, second, and third cycle irradiated and annealed samples. The results showed that the density of both electron and hole traps was found to decrease with increasing annealing temperature. For example, the density of electron trap for the first cycle sample was decreased from $8.8x10^{12}$ cm^{-3} for the unannealed sample to $4x10^{12}$ cm^{-3} for the 300° C annealed sample; for the hole trap it decreases from $1.1x10^{13}$ to $7x10^{12}$ cm^{-3}. For the third cycle annealed samples, the density of electron trap was decreased from $5.3x10^{13}$ for the unannealed sample to $8x10^{12}$ cm^{-3} for the 400° C annealed sample. Thus, reduction of defect density by a factor of 2 to 6 can be achieved through low temperature periodic annealing process. Fig. 4.29 shows the defect density for the E_c-0.71 and E_v+0.18 eV levels vs. the proton fluence for the unannealed and 200, and 300 °C annealed samples. The results showed that density of both E_c-0.71 eV and E_v+0.18 eV traps was found linearly increased with increasing proton fluence for the unannealed and 200° C annealed samples, as well as for the 300 °C annealed samples. In addition to the periodic thermal annealing and irradiation study, we have also studied the DLTS spectra for the nonperiodically annealed and irradiated samples (i.e., these samples were irradiated once with proton

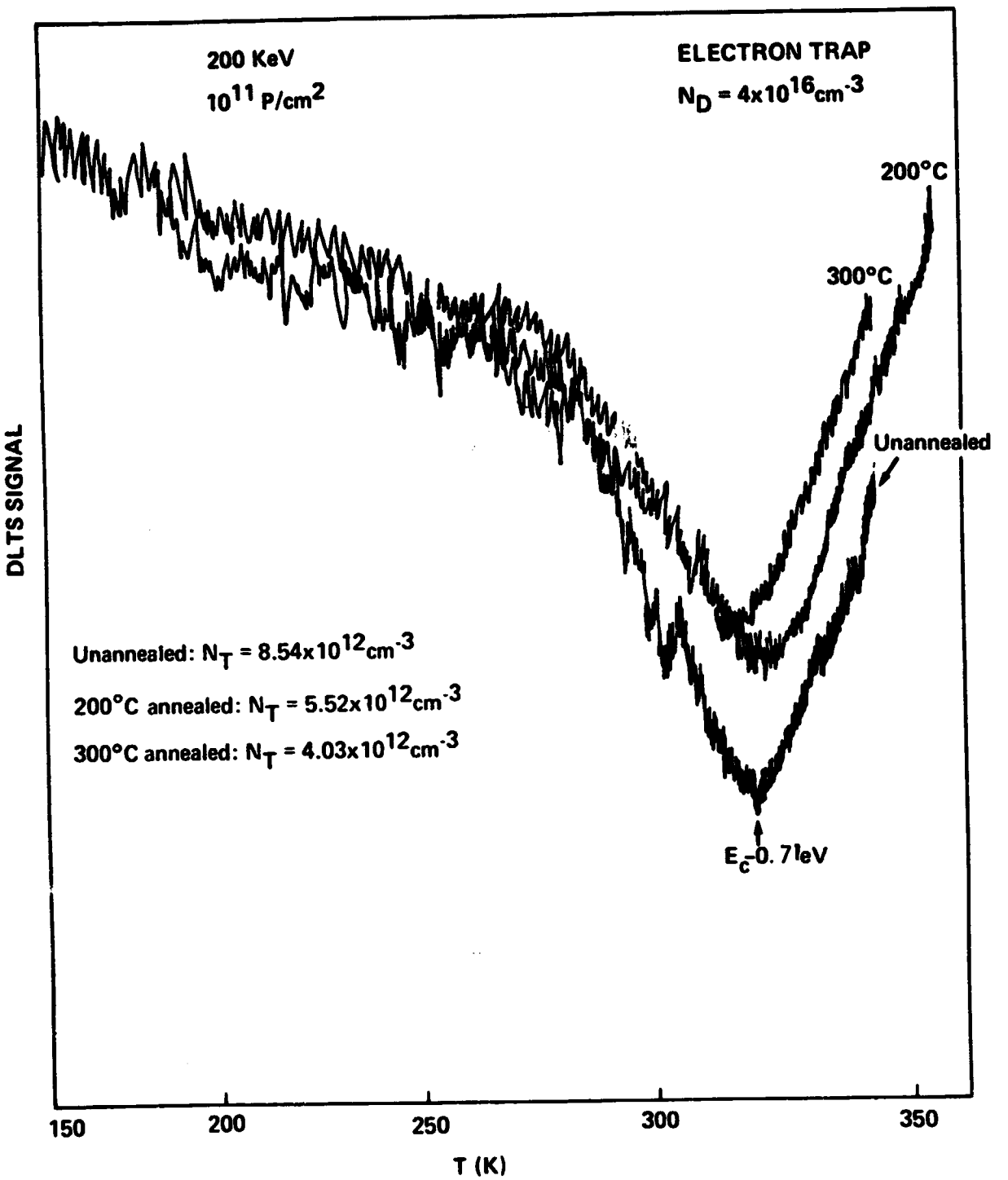

Fig. 4.20 DLTS scans of electron trap vs. annealing temperature for E_p = 200 KeV, ϕ_p = 1x10^{11} P/cm^2.

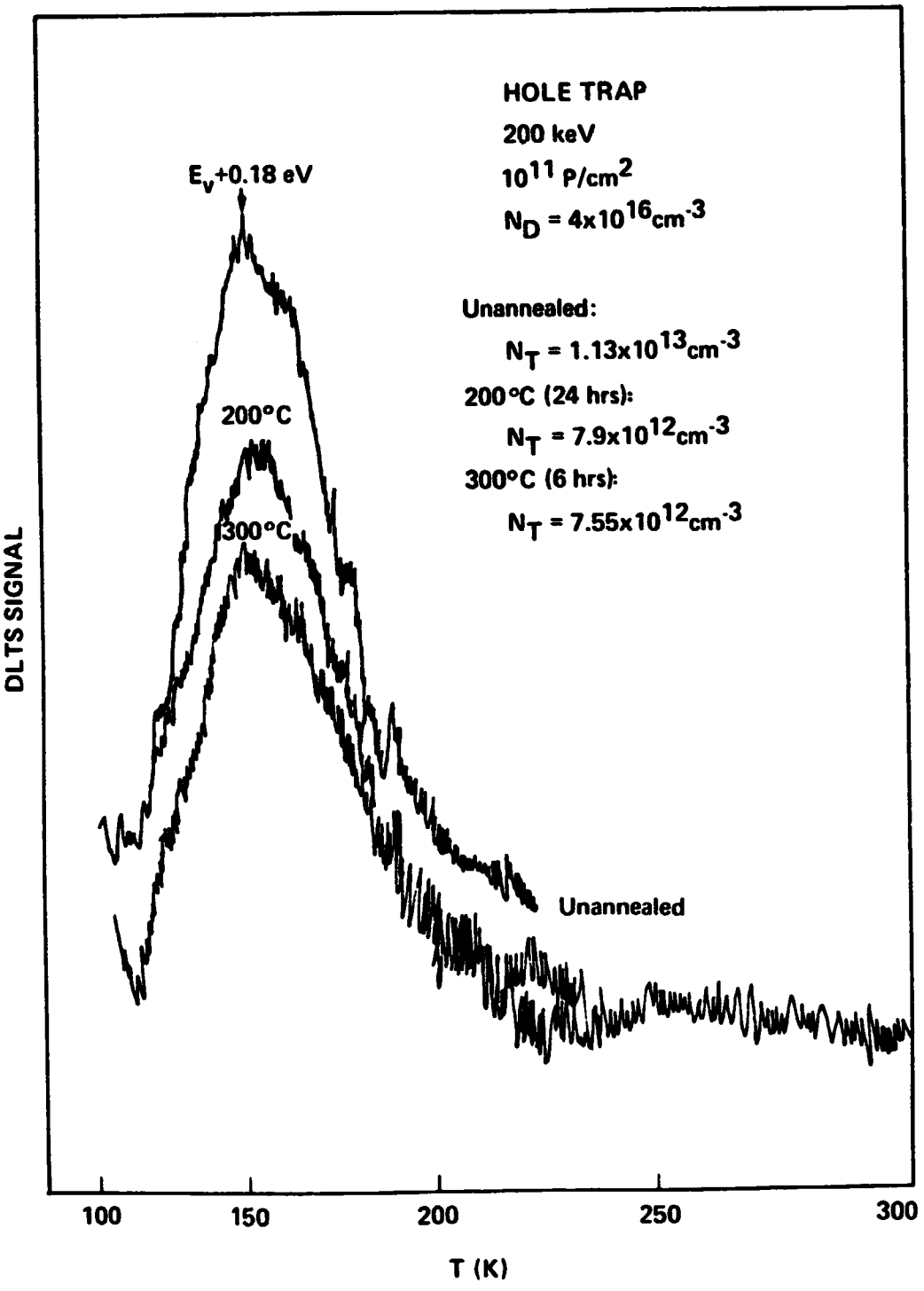

Fig. 4.21 DLTS scans of hole trap vs. annealing temperature for E_p = 200 KeV, ϕ_p = $1x10^{11}$ P/cm^2.

Fig. 4.22 DLTS scans of electron trap vs. annealing temperature for E_p = 200 KeV, $\phi_p = 2 \times 10^{11}$ P/cm^2.

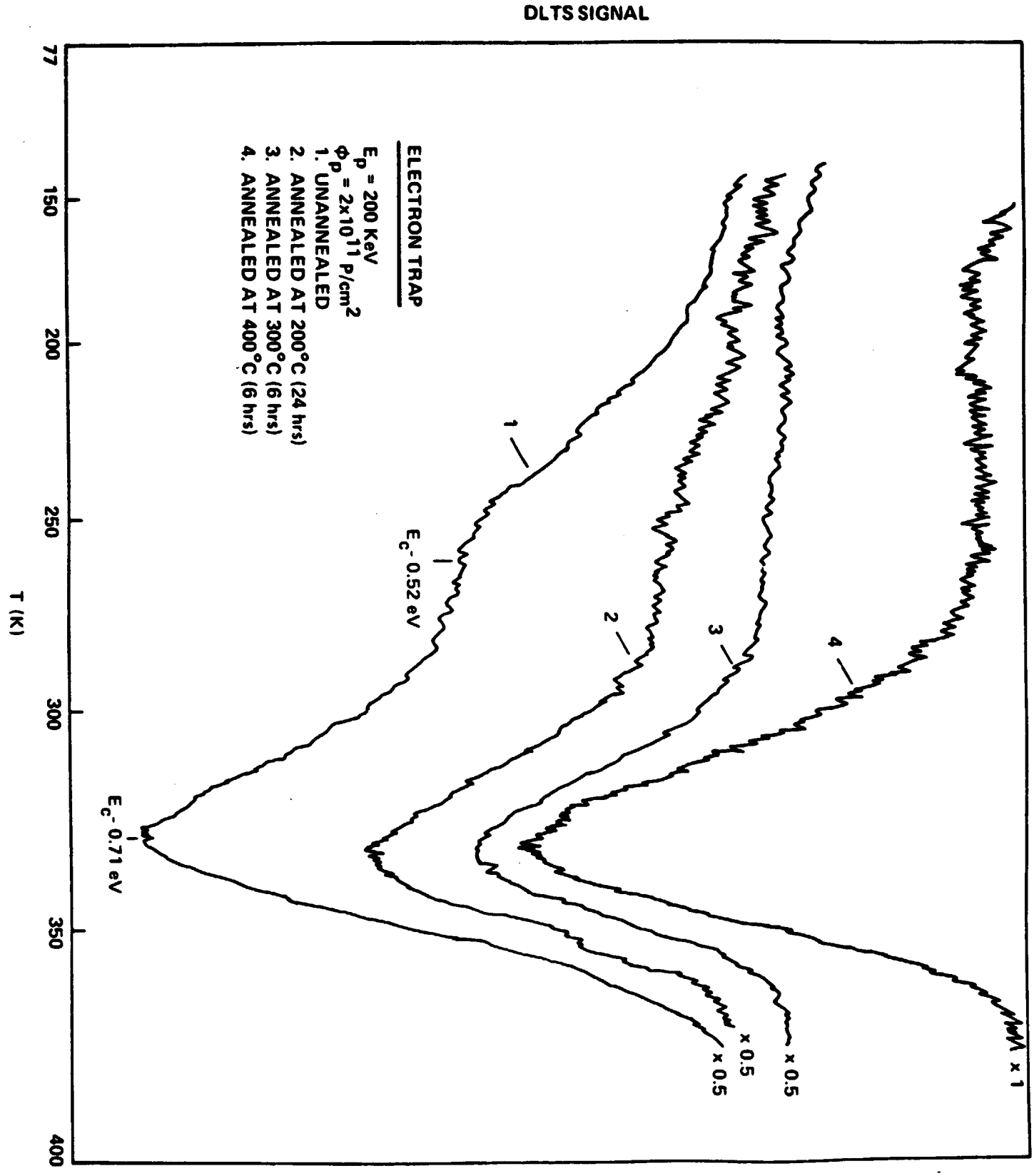

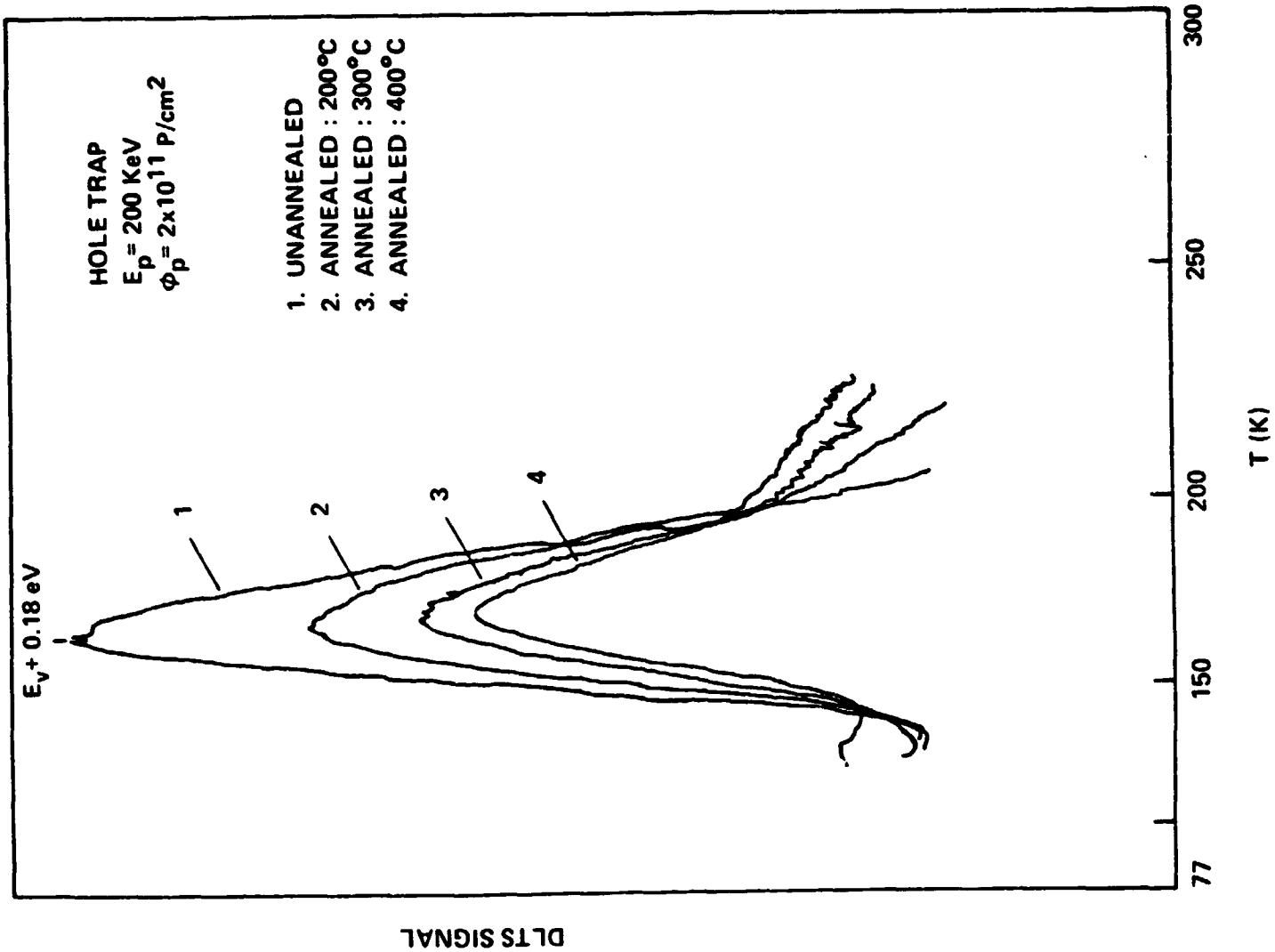

Fig. 4.23 DLTS scans of hole trap vs. annealing temperature for E_p = 200 KeV, ϕ_p = 2x10^{11} P/cm^2.

Fig. 4.24 DLTS scans of electron trap vs. annealing temperature for E_p = 200 KeV, ϕ_p = $3x10^{11}$ P/cm^2.

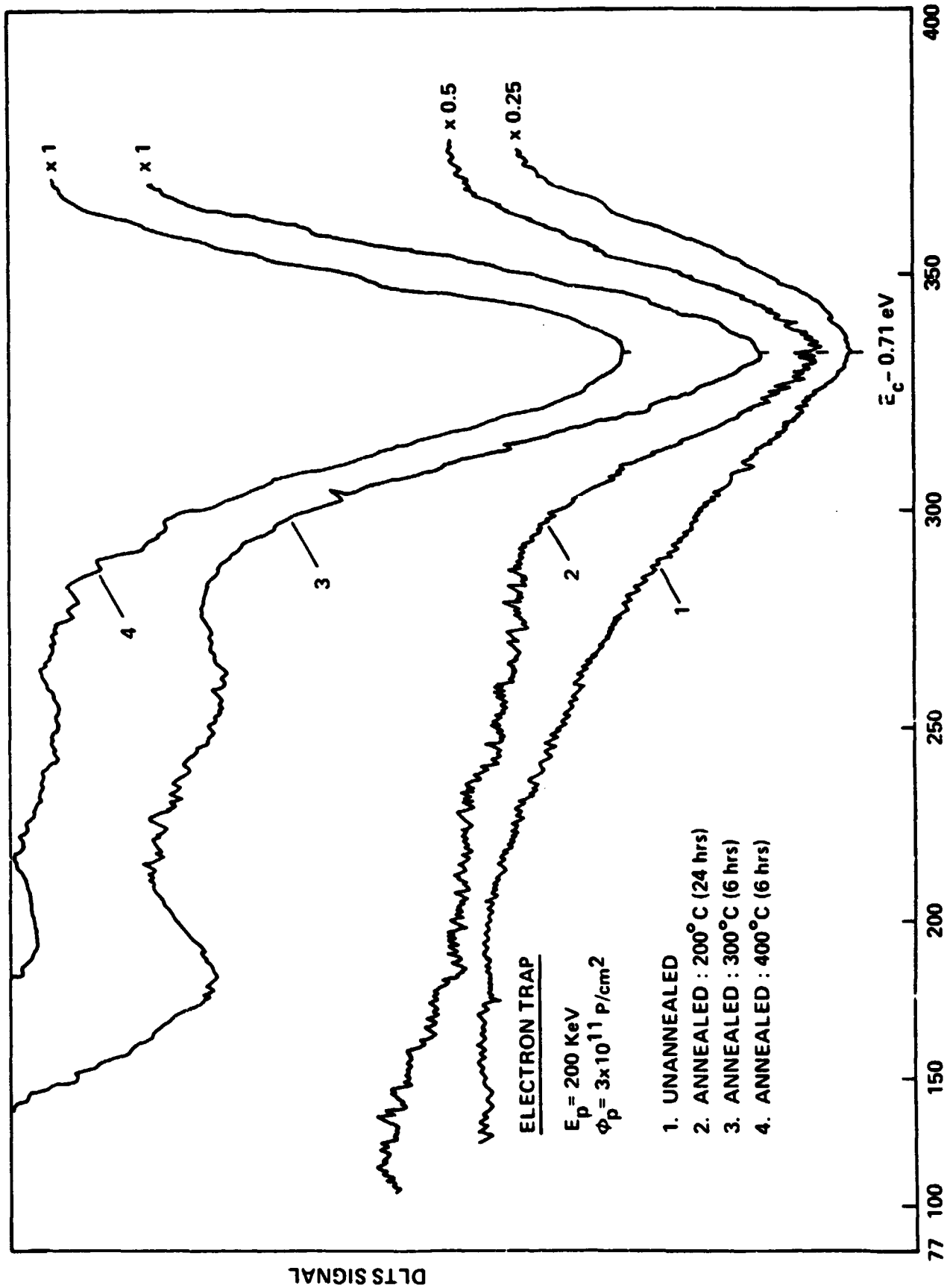

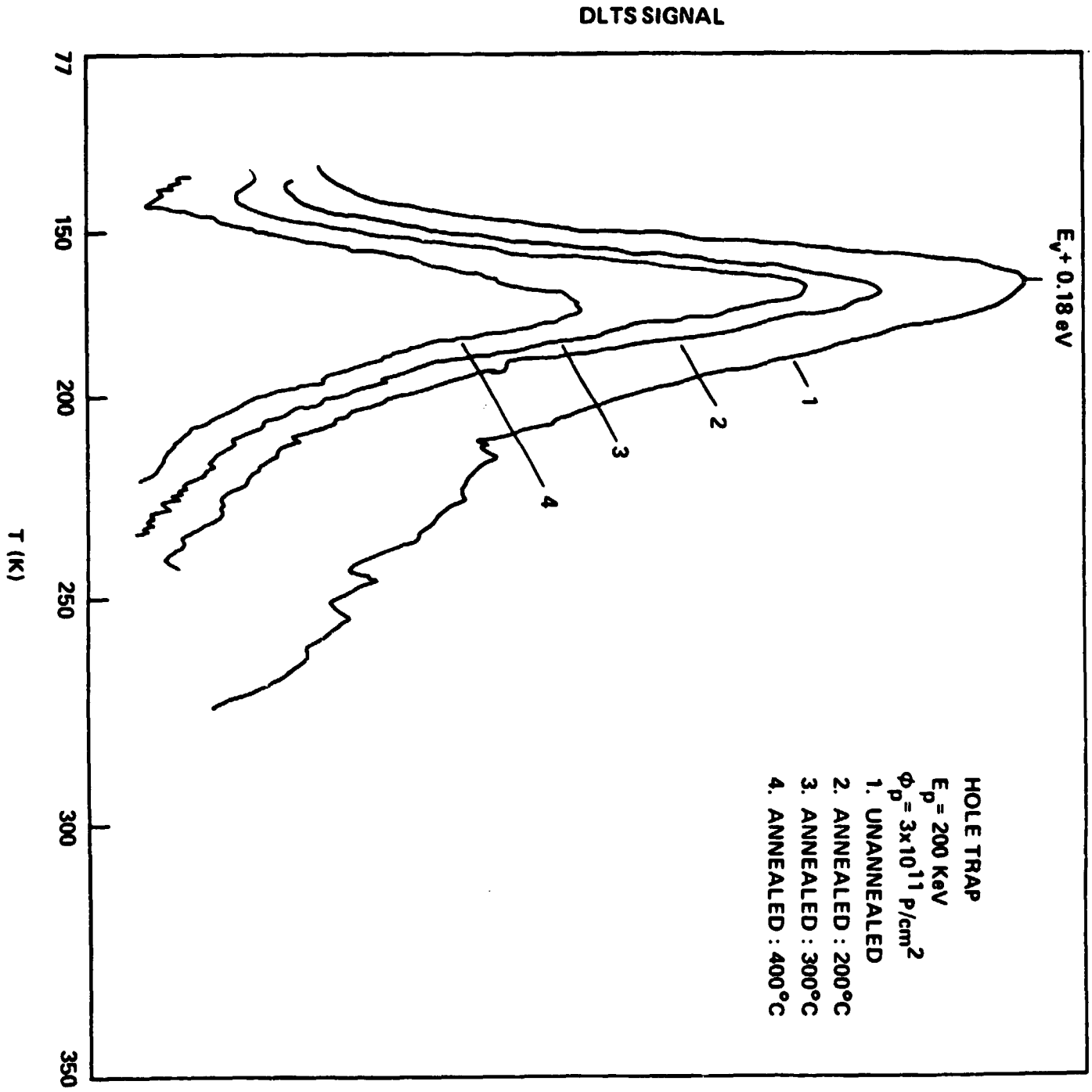

Fig. 4.25 DLTS scans of hole trap vs. annealing temperature for E_p = 200 KeV and ϕ_p = 3x10^{11} P/cm^2.

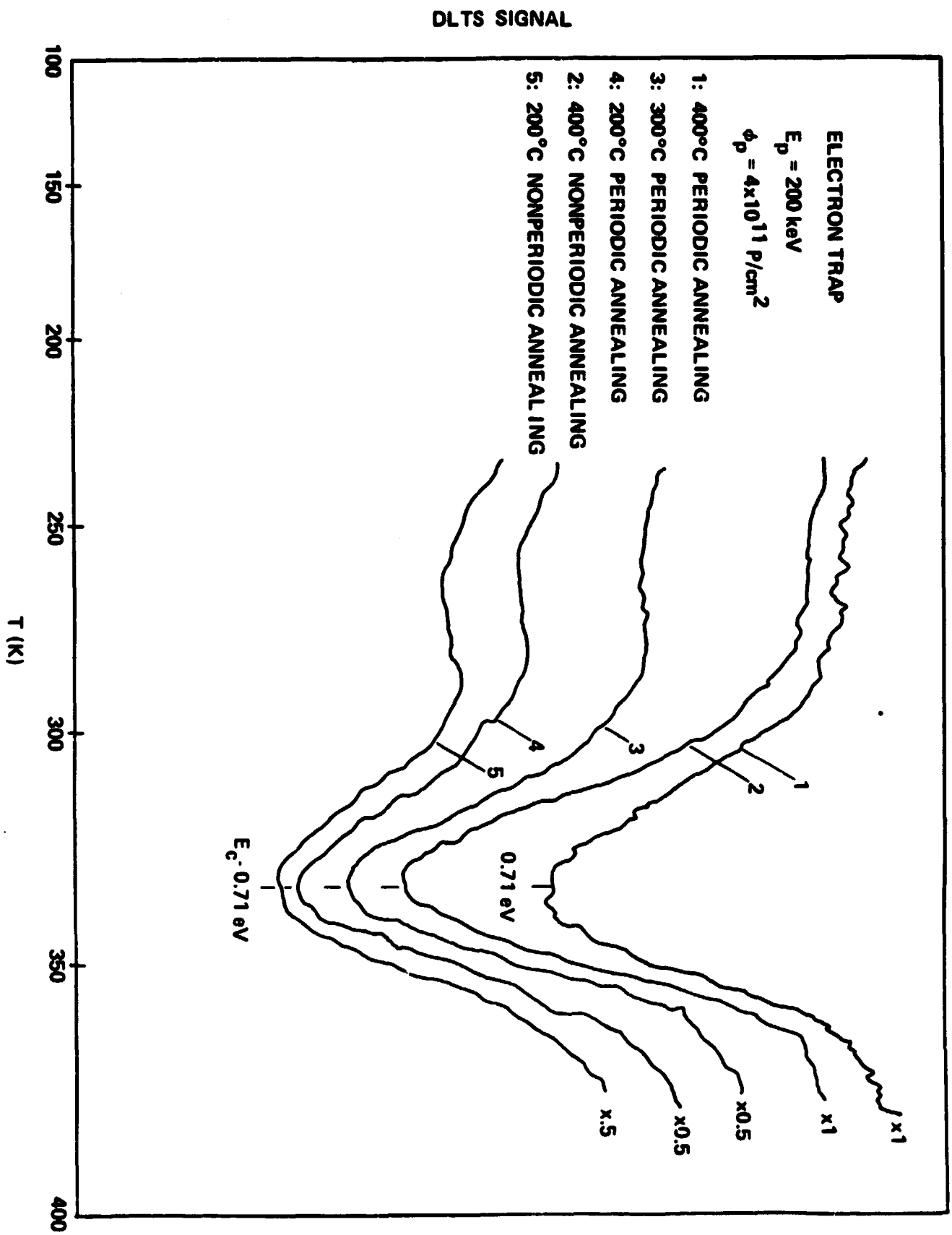

Fig. 4.26 DLTS scans of electron trap vs. annealing temperature for E_p = 200 KeV and ϕ_p = 4x10^{11} P/cm^2.

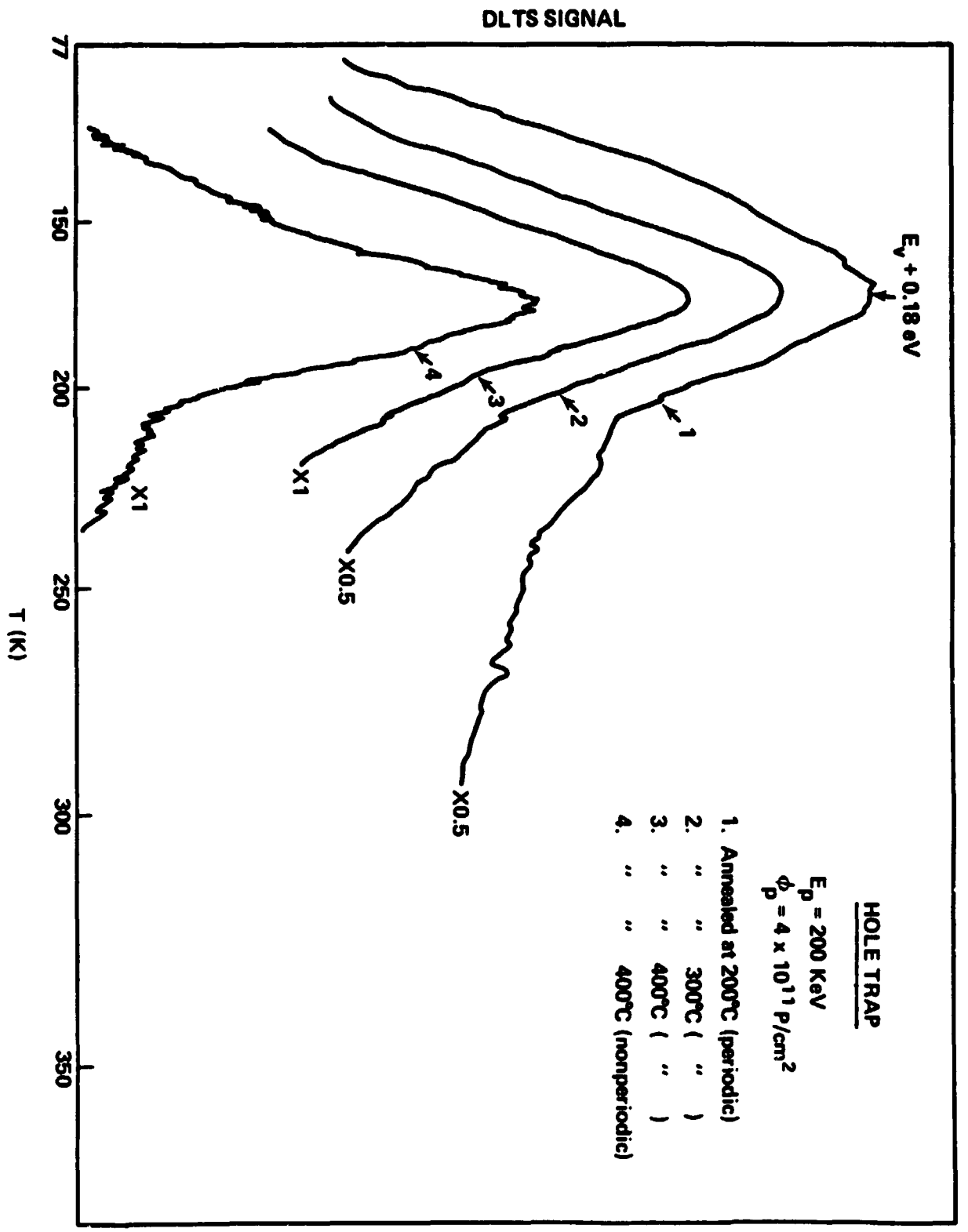

Fig. 4.27 DLTS scans of hole trap vs. annealing temperature for E_p = 200 KeV and $\phi_p = 4 \times 10^{11}$ P/cm^2.

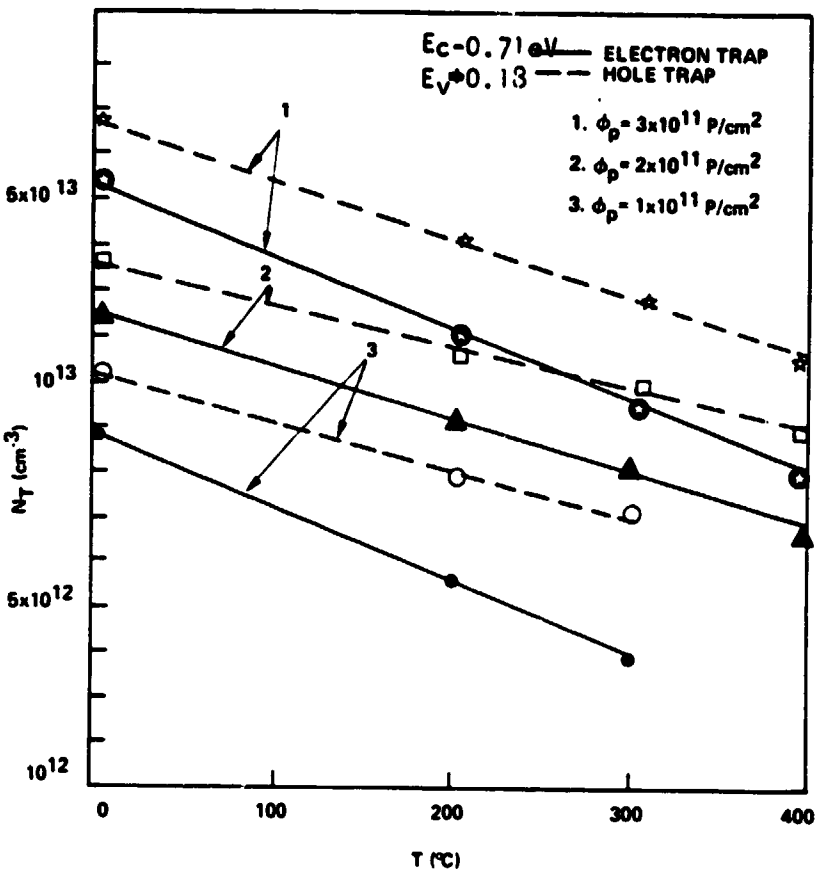

Fig. 4.28 Density of electron trap and hole trap vs. annealing temperature for the first, second, and third cycle 200 KeV proton irradiated samples.

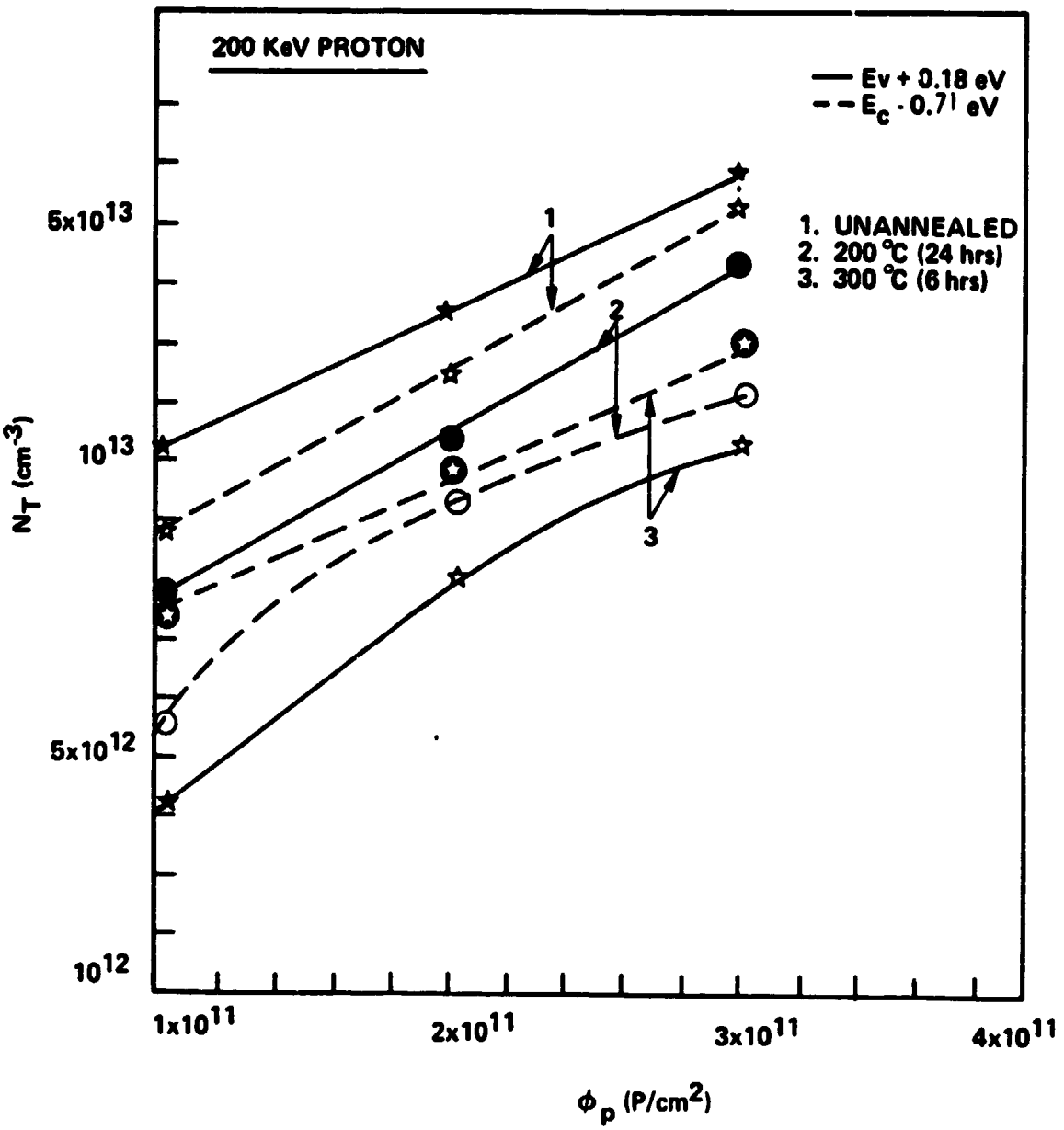

Fig. 4.29 Density of electron and hole trap vs. proton fluence for T_A = 0, 200 and 300° C.

fluence of $4x10^{11}$ P/cm^2 and annealed once at 200, 300, and 400 °C, respectively), Table 4.2 lists a comparison of the defect density between the fourth cycle periodically annealed and nonperiodically annealed samples for annealing temperatures of 200, 300, and 400 °C. No significant difference in defect density was observed in both cases. Table 4.3 lists the performance parameters of the periodic thermal annealed AlGaAs-GaAs solar cells irradiated by 200 KeV protons, as reported by HRL. It is noted that the defect profile for both electron trap (i.e. E_c-0.71 eV) and hole trap (E_v+0.18 eV) is not constant across the active region of the undoped n-GaAs layer, as are shown in Fig. 4.30 and Fig. 4.31, respectively. Fig. 4.30 shows the DLTS scans of electron trap, E_c-0.71 eV level, for three different reverse biased conditions (i.e., V_R = -2, -4, and -6V). The results showed that the defect density is highest near the edge of the junction and decreases with increasing distance in the undoped n-GaAs layer. A similar spatial distribution was also observed for the shallower electron trap, E_c-0.52 eV. On the contrary, the E_v+0.18 eV hole trap has an opposite spatial distribution; it has the lowest defect density near the edge of the junction space charge region and increases with increasing distance from the junction of the n-GaAs LPE layer. Thus, the physical origins of these electron and hole traps may be quite different. Based on the analysis given in section 3.1, the most likely candidate for the E_c-0.71 eV level may be due to the As_{Ga} or Ga_{As} antisite defect, and the possible candidate for the E_v+0.18 eV hole trap may be due to the V_{Ga} related defect. The E_v+0.18 eV level has constantly been observed in the $Al_xGa_{1-x}As$ LPE materials.

In short, from the study of the DLTS data for the periodically thermal annealed samples, it is concluded that periodic thermal annealing performed at 200, 300, and 400° C can effectively reduce the defect density for both E_c-0.71 eV electron trap and E_v+0.18 eV hole trap. Both the defect density and dark recombination current in the periodically annealed samples irradiated by 200 KeV protons decrease with

Table 4.2 Density of Electron and Hole Traps vs. Annealing Temperature in 200 keV proton Irradiated AlGaAs-GaAs Solar Cells ($\phi_p = 4x10^{11}$ P/cm^2).

Electron Trap Density (cm^{-3}) (E_c-0.71 eV)			Hole Trap Density (cm^{-3}) (E_v+0.18 eV)	
T (°C)	periodic annealing	non-periodic annealing	periodic annealing	non-periodic annealing
200	$3.23x10^{13}$	$2.91x10^{13}$	$5.34x10^{13}$	$5.82x10^{13}$
300	$2.24x10^{13}$	-	$3.57x10^{13}$	-
400	$9.8x10^{12}$	$1.62x10^{13}$	$2.2x10^{13}$	$2.4x10^{13}$

Table 4.3
Effect of Periodic Annealing on the
AlGaAs-GaAs Solar Cell Performance Parameters

Comments	Cell #	fluence	Annealing temp.	Annealing time	I_{sc} (ma)	V_{oc} V	F.F.	P_m (mw)	N_c (%)	P/P_o %
First Cycle annealing & irradiation	5549	0	0	0	114	1.0	0.75	85.3	15.8	100%
	5549	$1x10^{11}$	0	0	90	0.84	0.74	55.8	10.3	65.3%
	5549	$1x10^{11}$	200°C	24	95	0.87	0.75	61.8	11.4	73%
	5552	$1x10^{11}$	300 °C	6	101	0.91	0.75	69	12.8	81%
	5556	$1x10^{11}$	400 °C	6	104	0.92	0.75	72	13.3	85%
Second Cycle annealing & irradiation	5549	$2x10^{11}$	0	0	79	0.83	0.74	48.3	8.9	56.3%
	5549	$2x10^{11}$	200 °C	20	89	0.86	0.75	57.2	10.6	67%
	5552	$2x10^{11}$	300 °C	6	96	0.90	0.75	65	12.0	76%
	5556	$2x10^{11}$	400 °C	6	100	0.91	0.74	67.3	12.4	77%
Third Cycle annealing & irradiation	5549	$3x10^{11}$	0	0	79	0.82	0.74	47.6	8.8	55.7%
	5549	$3x10^{11}$	200 °C	20	87.5	0.85	0.74	55.3	10.2	64.6%
	5552	$3x10^{11}$	300 °C	6	90	0.88	0.75	59	10.9	69%
	5557	$3x10^{11}$	400 °C	6	99	0.91	0.73	66.1	12.2	76%
Fourth Cycle annealing & irradiation	5549	$4x10^{11}$	0	0	80	0.81	0.73	47.5	8.8	55.7%
	5549	$4x10^{11}$	200 °C	5	85	0.84	0.73	52.4	9.7	61.4%
	5552	$4x10^{11}$	300 °C	6	86.5	0.86	0.75	56.1	10.4	66%
	5556	$4x10^{11}$	400 °C	6	93	0.91	0.75	63	11.6	74%

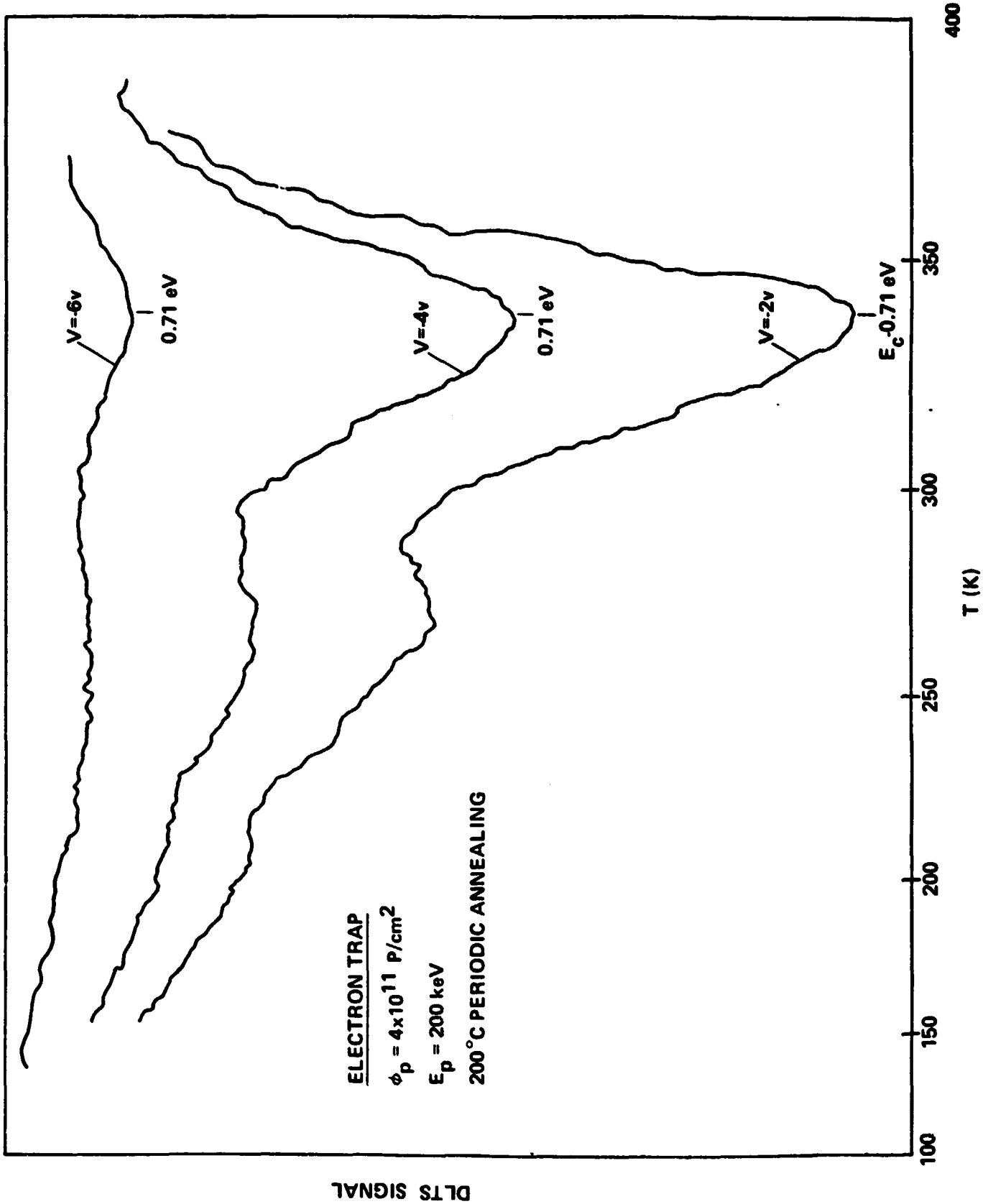

Fig. 4.30 DLTS scans of electron trap vs, reverse biased voltage, for E_p = 200 KeV, ϕ_p = $4x10^{11}$ P/cm^2 and T_A = 200° C.

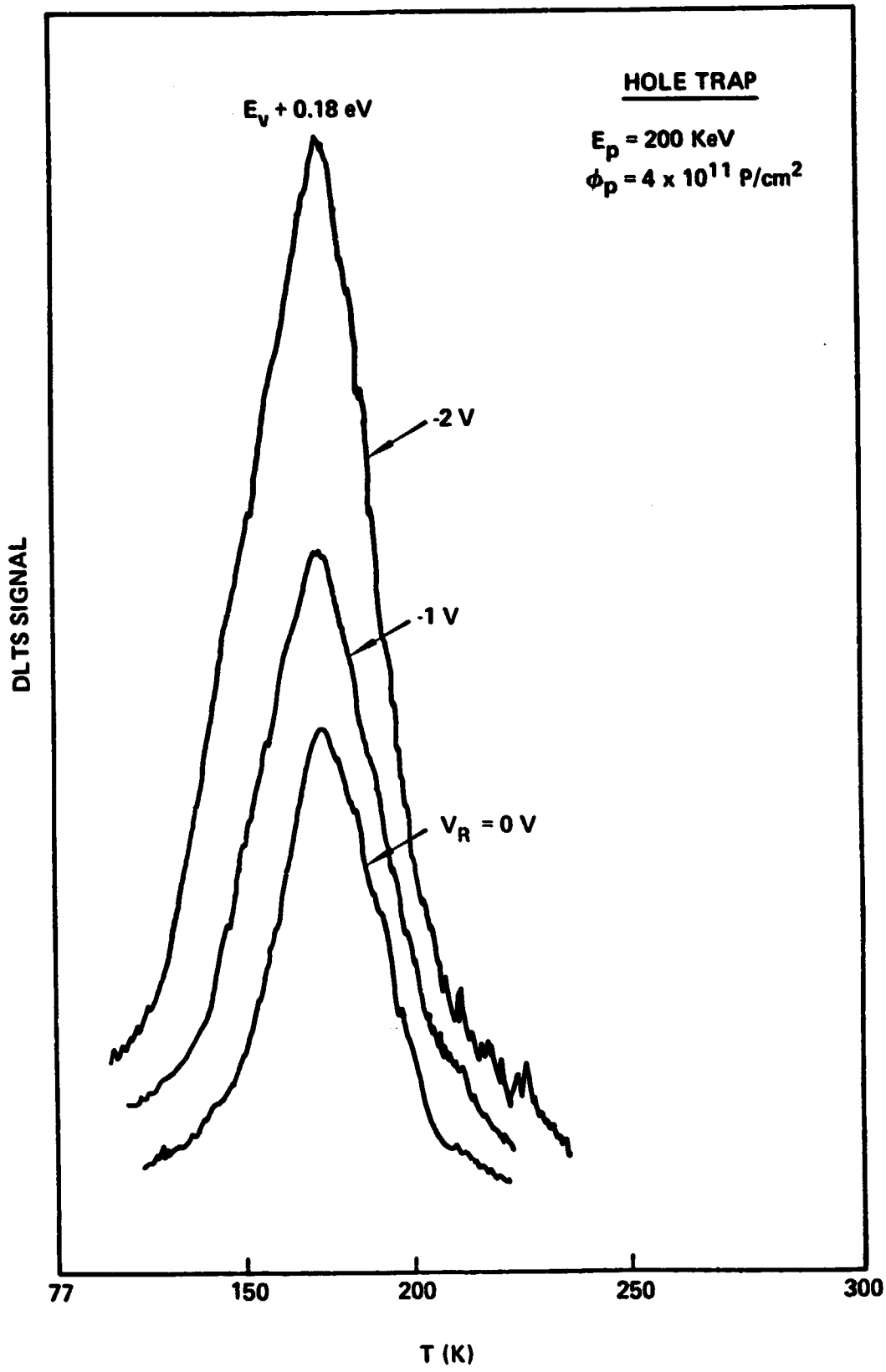

Fig. 4.31 DLTS scans of hole trap vs. reverse biased voltage, for E_p = 200 KeV, Φ_p = 4x10^{11} P/cm^2.

increasing annealing temperature. The periodic thermal annealing appears to have a slight edge over the non-periodic annealing process in terms of reducing the defect density and dark current in the 200 KeV proton irradiated GaAs solar cells.

4.3 Hole Diffusion Lengths, Damage Coefficients, and other Recombination Parameters in the Low Energy Proton Irradiated GaAs Solar Cells.

In addition to the I-V, C-V, and DLTS measurements discussed in the previous sections, we have also conducted the SEM-EBIC measurements on the low energy proton irradiated GaAs solar cells to determine the hole diffusion lengths in the undoped n-GaAs LPE layers. Fig. 4.32 shows a schematic diagram of a semiautomaticSEM-EBIC set-up for diffusion length measurements. Fig. 4.33 shows a typical trace of SEM-EBIC scans across the cleave plane of a AlGaAs-GaAs mesa diode. Fig. 4.34 shows the SEM-EBIC current vs. distance, x, for the low energy proton irradiated AlGaAs-GaAs solar cells irradiated by different proton energies and fluences. The effective hole diffusion length is deduced from the slope of the log I_{sc} vs. x plot. Fig. 4.35 shows the hole diffusion lengths vs. proton fluence for 50, 100, and 290 KeV samples. Table 4.4 summarizes the measured defect and recombination parameters in the low energy proton irradiated AlGaAs-GaAs solar cells. Table 4.5 lists the measured hole diffusion lengths and the calculated damage coefficients for the low energy proton irradiated GaAs solar cells studied in this research program. As can be seen from Tables 4.4 and 4.5 that the hole diffusion lengths measured by SEM-EBIC method are in good agreement with those deduced from forward I-V data. The damage coefficients calculated from the hole diffusion length data for the low energy proton irradiated GaAs cells vary between 1 to 2×10^{-4} for proton fluences of 10^{11} and 10^{12} P/cm^2. These values are about a few times higher than those reported by Anspaugh for the 8.3 MeV ($K_p = 9.1\times10^{-5}$ to 2.0×10^{-5}) and 17.5 MeV ($K_p = 5.4\times10^{-5}$ to 1.2×10^{-5}) proton irradiated GaAs solar cells. However, this appears to be reasonable since the low energy protons are expected to create more damages to the GaAs solar cell structure used in this study than those of medium and high energy

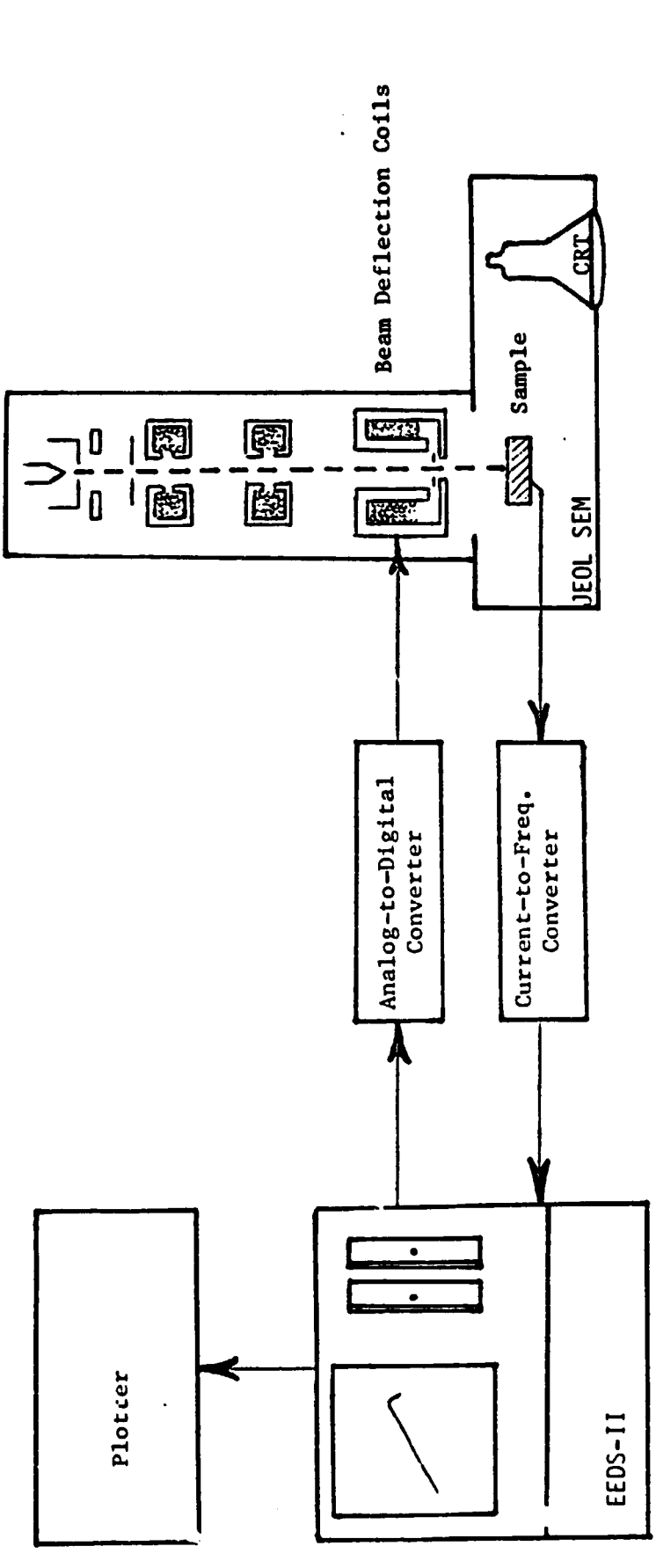

Fig. 4.32 Schematic diagram of a semiautomatic SEM-EBIC set-up for diffusion length measurement

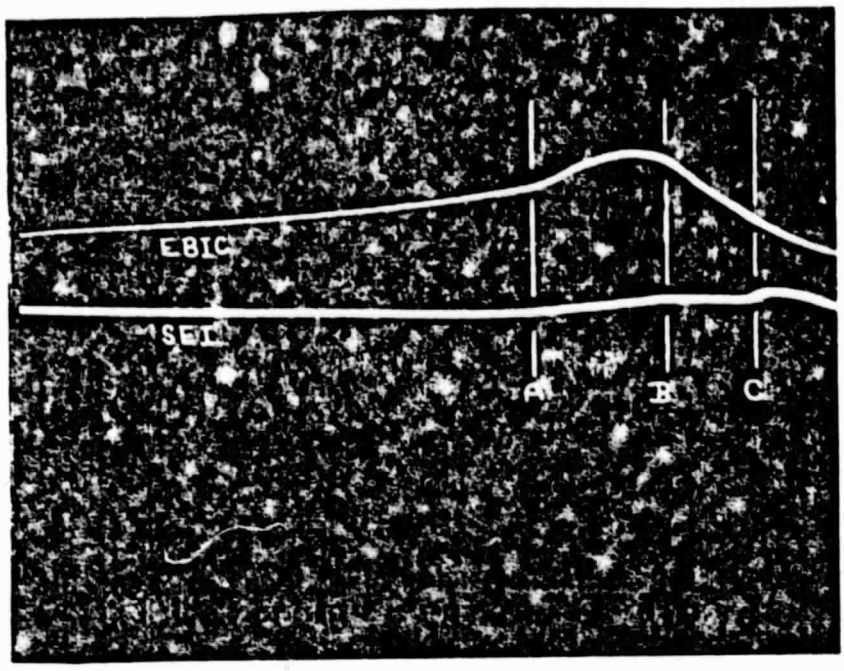

(a) Trace of EBIC and SEI (secondary electron image) curves across the same line perpendicular to the p-n junction

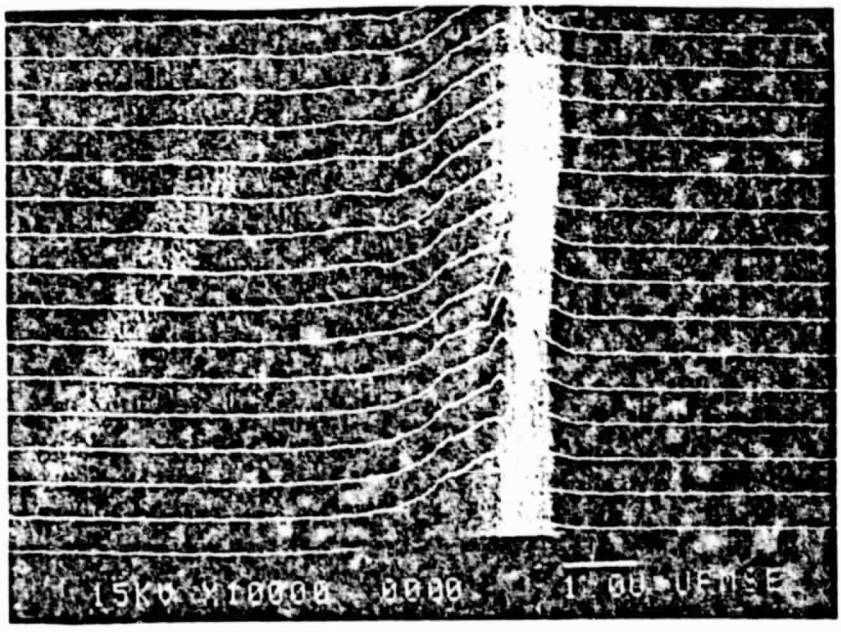

(b) Multiple exposure of SEI of cleaved diode surface and EBIC curves.

Fig. 4.33 SEM-EBIC scans across an AlGaAs-GaAs diode.

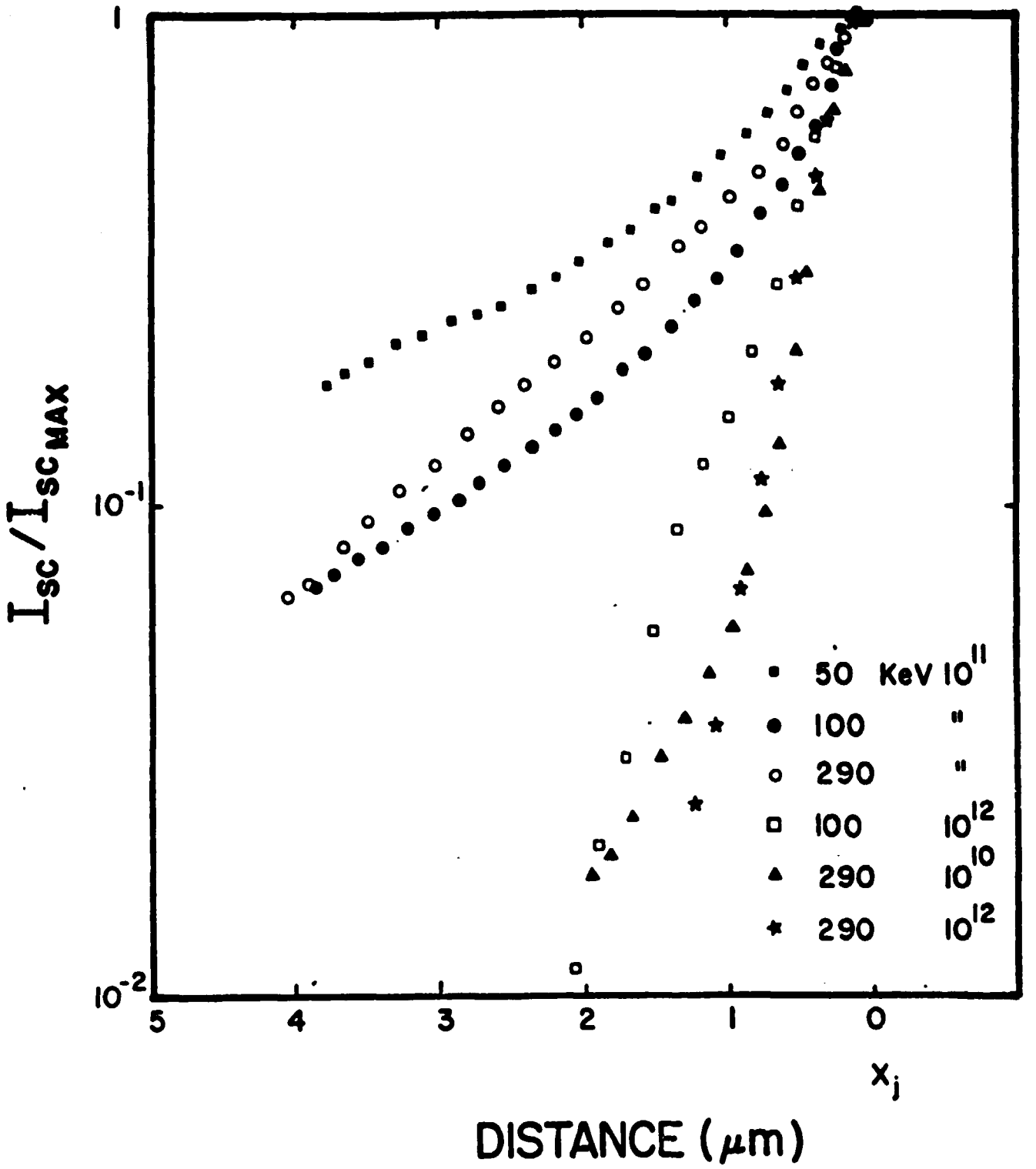

FIG. 4.34 SEM-EBIC CURRENT VERSUS DISTANCE X FOR ALGAAS-GAAS MESA DIODES IRRADIATED BY PROTONS WITH DIFFERENT ENERGIES AND FLUENCES.

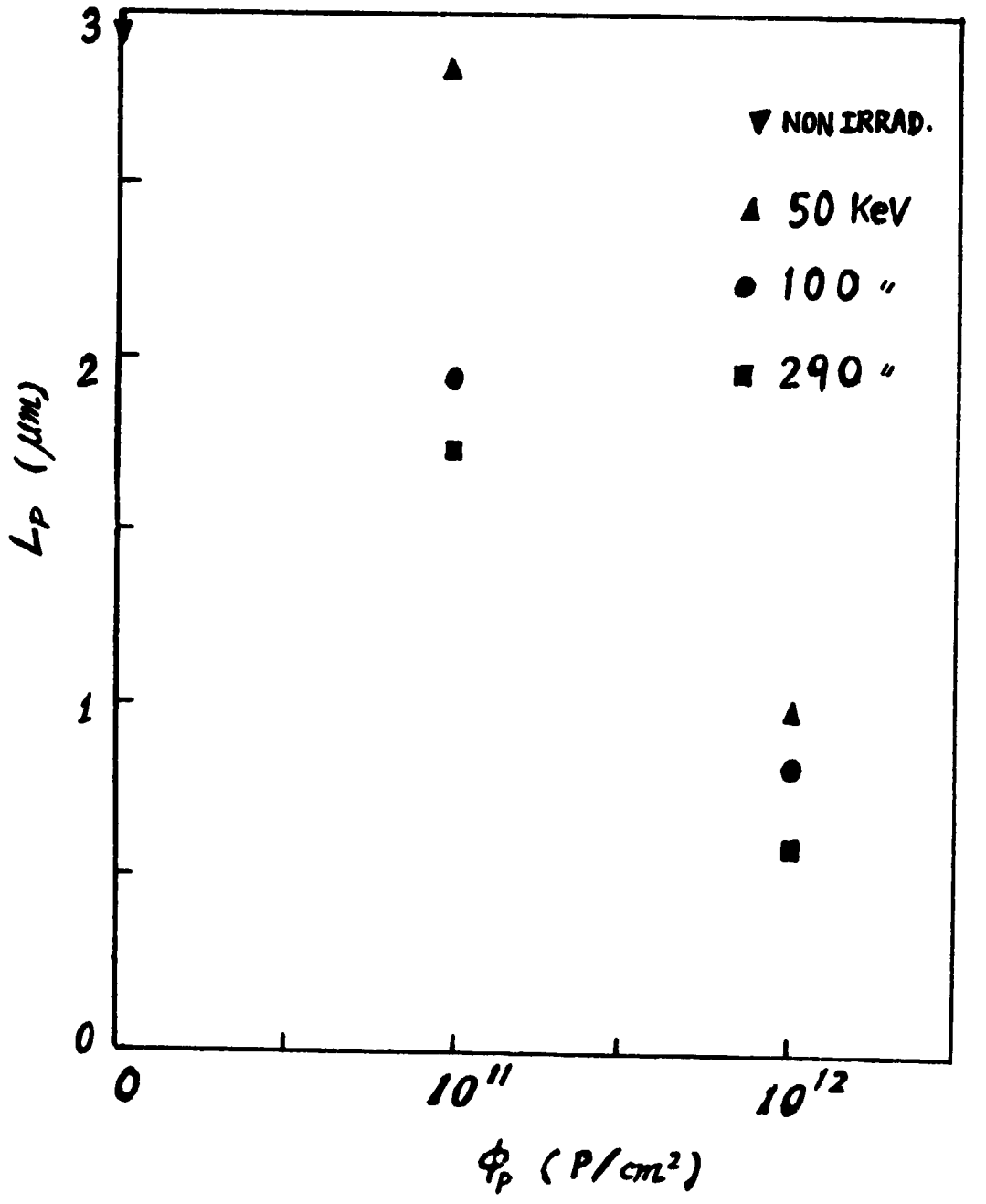

Fig. 4. 35 Hole diffusion length vs proton fluence for the low energy proton irradiated GaAs solar cells as determined by the SEM-EBIC techniques.

Table 4.4 Hole Diffusion Lengths and Damage Coefficients in Low Energy Proton Irradiated AlGaAs-GaAs Solar Cells

Proton Energy KeV	Fluence (P/cm^2)	Hole diffusion length (μm)	Damage constant
50	10^{11}	2.73	9.31×10^{-6}
100	10^{11}	1.97	1.33×10^{-4}
"	10^{12}	0.86	1.11×10^{-4}
290 KeV	10^{11}	1.72	2.13×10^{-4}
"	10^{12}	0.67	2.1×10^{-4}

Table 4.5 Measured defect and recombination parameters in low energy proton irradiated AlGaAs-GaAs diodes.

Proton energy (KeV)	Proton fluence (P/cm^2)	Trap Level Electron (E_t) eV	Trap Level Hole (E_t) eV	Trap Density Electron (cm^{-3})	Trap Density Hole (cm^{-3})	Capture cross section Electron $\sigma_n(cm^2)$	Capture cross section Hole $\sigma_p(cm^2)$	Hole diffusion length (From DLTS) L_p (μm)	Hole diffusion length (From EBIC) L_p (μm)	Effective diffusion length (From I-V curve L(μm))
0	0	--	--	--	--	--	--	--	2.83	3.1
50	10^{11}	--	--	--	--	--	--	--	2.73	2.6
	10^{12}	--	--	--	--	--	--	--	--	0.93
		--	--	--	--	--	--	--	--	
100	10^{11}	0.2	0.17	1.64×10^{13}	5.63×10^{12}	1×10^{-16}	5.9×10^{-18}	1.73	1.97	2.3
		0.71	0.71	2.3×10^{13}	1.09×10^{13}	2.2×10^{-13}	1.2×10^{-12}			
290	10^{11}	0.20	0.17	7.7×10^{12}	5.2×10^{12}	--	--			
		0.71	0.71	1.2×10^{13}	1.2×10^{13}	2.2×10^{-13}	1.6×10^{-12}	1.44	1.72	1.6
100	10^{12}	0.14	--	4.9×10^{13}	--	1.2×10^{-15}	--			
		0.31	0.44	1.5×10^{14}	8.4×10^{13}	3.8×10^{-15}	9×10^{-15}	0.90	0.86	0.8
		0.52	0.57	2.6×10^{14}	2×10^{14}	1.3×10^{-14}	2×10^{-13}			
290	10^{12}	0.11	--	2.4×10^{13}	--	8.9×10^{-14}	--			
		0.31	0.44	2.2×10^{14}	1.9×10^{14}	8×10^{-15}	9.3×10^{-15}	0.84	0.67	0.57
		0.71	0.57	3.4×10^{14}	2.4×10^{14}	1.3×10^{-13}	2.3×10^{-13}			

protons, as discussed earlier.

V. CONCLUSIONS

Study of radiation induced deep-level defects and recombination properties in proton irradiated AlGaAs-GaAs solar cells fabricated at HRL has been carried out in this research program. Detailed analysis of the defect and recombination parameters in the proton irradiated GaAs solar cells has been made for a wide range of proton energy (i.e., 50 KeV, 100 KeV, 200 KeV, 290 KeV, 800 KeV, 1 and 10 MeV) and proton fluences (i.e., 10^{11}, $5x10^{11}$, 10^{12}, 10^{13} P/cm^2). Experimental tools such as I-V, C-V, DLTS, and SEM-EBIC techniques have been employed to deduce the defect and recombination parameters in these proton irradiated samples. In addition, a systematic study of the low temperature (200 to 400° C) periodic thermal annealing behavior of deep-level in defects in the 200 KeV proton irradiated GaAs solar cells has also been made in this work. The main condlusions obtained from this study are: (1) Among all proton energies studied, the 200 and 290 KeV protons produced the highest damages and defect density in the GaAs solar cell structure studied, (2) low temperature thermal annealing (200 to 400° C) process is beneficial for reducing defect density and dark recombination current, and is capable of recovering the power loss in the proton irradiated GaAs solar cells, (3) good correlation between our measured defect parameters and solar cell performance parameters has been obtained for the 200 and 290 KeV proton irradiated GaAs solar cells, (4) in the periodic thermal annealing study of the 200 KeV proton irradiated samples, the defect density was found decreased linearly with increasing annealing temperatures and increased with increasing proton fluence (from 10^{11} to $4x10^{11}$ P/cm^2), (5) the observed energy levels for electron traps include E_c-0.11, 0.14, 0.20, 0.31, 0.52, 0.60, and 0.71 eV, and for hole traps, E_v+0.17, 0.29, 0.41, 0.52, 0.57, and 0.71 eV, for proton energies of 100 KeV to 10 MeV and fluences of 10^{11} to 10^{13} P/cm^2, (6) most of the deep-level defects observed in these proton

irradiated GaAs samples are believed to be due to vacancy, interstitial and antisite related native defects; identification of these defect is extremely difficult and required further studies, (7) the observed deep-level defects such as E_c-0.60 or 0.71 eV electron traps and E_v+0.52 and 0.71 eV hole traps are effective recombination centers in these proton irradiated GaAs LPE layers, (8) hole diffusion lengths in the undoped n-GaAs layer were found to vary between 3 μm for the unirradiated GaAs and 0.3 μm for the 290 KeV proton irradiated samples with 10^{13} P/cm^2 proton fluences, (9) damage constants for the low energy proton irradiated samples are varied between 1 and $2x10^{-4}$, (10) comparing periodic and non-periodic thermal annealing process no significant difference in defect density was observed in these 200 KeV proton irradiated samples.

In short, from the results of this study, a better understanding of the radiation induced deep-level defects in the proton irradiated AlGaAs-GaAs solar cells has been obtained in this research program. Low temperature thermal annealing study, aimed at reducing defect density and recovering power loss in GaAs solar cells due to proton irradiation, has yielded useful information for improving the solar cell performance in the radiation environment. A similar study for the one-MeV electron irradiation in GaAs solar cells should be taken for the future work.

VI. TECHNICAL REPORTS, PUBLICATION AND CONFERENCE PAPERS

1. S. S. Li, "Electronic Properties of Defects Induced by One-MeV Proton Irradiation in GaAs," NASA Semi-annual Technical Report, Sept., 1978. Grant No. NSG-1425.

2. S. S. Li, "Electronic Properties of Defects in Low Energy Proton Irradiation in AlGaAs-GaAs Solar Cells," NASA Semi-annual Technical Report, Sept. (1979).

3. S. S. Li, "Defect and Electronic Properties of Proton Irradiated AlGaAs-GaAs Solar Cells," NASA Semi-annual Technical Report, Sept. (1980), Grant No. NSG-1425.

4. S. S. Li, D. W. Schoenfeld, F. Llevada, and K. L. Wang, "Defects Induced by one-MeV Proton Irradiated n-GaAs," Proc. of the International Conference on Recombination in Semiconductors," Solid-State Electronics, vol. 21, p. 1616 (1978). Paper presented at the ICRS at University of Southampton, England, August 29-31 (1978).

5. S. S. Li, D. W. Schoenfeld, and K. L. Wang, "Detection of Deep-level Defects in one-MeV Proton Irradiated GaAs solar cells using DLTS Methods," Proc. IEEE 13th Photovoltaic Specialists Conference, p. 465, Washington, D.C., June (1978).

6. S. S. Li, et. al., "Deep Level Defects and Diffusion Length Measurements in Low Energy Proton Irradiated GaAs," paper presented at the 21st Electronic Material Conference, Boulder, Colorado, June 27-29 (1979); J. Electronic Material, v. 9, No. 2, pp. 335-352 (1980).

7. S. S. Li, et. al., "Deep-level Defects, Recombination Mechanisms and Their Correlation to the Performance of AlGaAs-GaAs solar cells Irradiated by Low Energy Protons," IEEE Trans. Electron Devices, ED-27, No. 4, pp. 857-864 (1980).

8. S. S. Li, et. al., "Electronic Properties of Deep-level Defects in Low Energy Proton Irradiated AlGaAs-GaAs Solar Cells," IEEE Proc. 14th Photovoltaic Specialists Conference, pp. 1080-84 (1980).

9. S. S. Li, et. al, "Effects of Thermal annealing on the Deep-level Defects and I-V Characteristics of 200 KeV Proton Irradiated AlGaAs-GaAs Solar Cells," Proc. of the 15th Intersociety Energy Conversion Engineering Conference., p. 343-359, Seattle, Washington, Aug. 18-22 (1980).

10. S. S. Li, et. al., "Defect Characterization and Thermal Annealing Study of 200 KeV Proton Irradiated n-GaAs LPE Layers," Proc. of the 11th International Conf. on Defects and Radiation Effects in Semiconductors, Sept. 7-11, Tokyo, Japan (1980).

11. S. S. Li, "Characterization of Deep-Level Defects Induced by Proton Irradiation in AlGaAs-GaAs Solar Cells," Proc. of the Fourth High Efficiency Radiation Damage Solar Cell Meeting, NASA Lewis Research Center, Oct. 15-17, (1980).

12. S. S. Li, "Study of Radiation Induced Deep-Level Defects and Annealing Effects in The Proton Irradiated AlGaAs-GaAs Solar Cells," Proc. 15th IEEE Photovoltaic Specialists Conf., Orlando, FL (1981).

13. S. S. Li, T. T. Chiu and R. Y. Loo, "Effects of Low Temperature Periodic Annealing on the Deep-Level Defects in 200 KeV Proton Irradiated AlGaAs-GaAs Solar Cells," 18th Annual Conference on Nuclear & Space Radiation Effects, Seattle, Washington, July 21-24 (1981).

Other Documentations:

1. One Ph.D. dissertation and four M.S. theses have been completed since 1978 which were supported by this research grant.

VII. REFERENCES

1. H. J. Hovel and J. M Woodall, "High Efficiency $Ga_{1-x}Al_xAs$-GaAs Solar Cells", Appl. Phys. Lett., Vol. 21, p. 379, 1972.

2. J. W. Corbett, "Study of Radiation Damage in Silicon", COMSAT Contract Technical Report, 1978.

3. S. S. Li, "Study of Electronic Properties in One-MeV Proton Irradiated GaAs", NASA Semiannual Technical Report, September, 1978.

4. S. S. Li, D. W. Schoenfeld, F. Llevada and W. Krull, "Defects Induced by One-MeV Proton Irradiated GaAs", Proc. of International Conference on Recombination in Semiconductors, Suppl. of Solid State Electronics., Dec., 1978.

5. S. S. Li, W. L. Wang, P. W. Lai, R. W. Owen, R. Y. Loo and S. G. Kamath, "Defects and Diffusion Length Measurements in n-GaAs Irradiated by Low Energy Protons", 21th Electronic Material Conference; to be published in J. of Electronic Materials, 1980.

6. S. S. Li, W. L. Wang, P. W. Lai, R. Y. Loo, S. G. Kamath and R. Knechtli, "Deep-Level Defects, Recombination Mechanisms, and Their Correlation to the Performance of Low Energy Proton Irradiated AlGaAs-GaAs Solar Cells", IEEE Trans. Electron Devices, Special Issue on Photovoltaic Devices, April issue, 1980.

7. R. Loo, S. Kamath, and R. Knechtli, "Low Energy Proton Radiation Damage to AlGaAs-GaAs Solar Cells", Final Report for period July 1978 to January 1979, NASA, 1979.

8. A. G. Foyt, W. T. Lindley, C. M. Wolfe, and J. P. Donnelly, "Isolation of Junction Devices in GaAs Using Proton Bombardment", Solid State Electron., vol. 12, p. 209, 1969.

9. H. Harada and M. Fujimoto, "Electrical Properties of Proton-Bombarded n-Type GaAs", Ion Implantation in Semiconduction, Plenum Publishing Corp., New York, p. 73, 1974.

10. J. J. Wysocki, P. Rappaport, E. Davison and J. J. Loferski, "Low-Energy Proton Bombardment of GaAs and Si Solar Cells", IEEE Transactions on Electronic Devices, vol. ED-13, p. 420, 1966.

11. D. V. Lang, "Review of Radiation-Induced Defects in III-V Compounds", Inst. Phys. Conf. Ser. No. 31, p. 70, 1977.

12. R. Loo, L. Goldhammer, B. Anspaugh, R. C. Knechtli, and G. S. Kamath, "Electron and Proton Degradation in (AlGa)As-GaAs Solar Cells", 13th IEEE Photovoltaic Specialists Conference, p. 562, 1978.

13. L. W. Aukerman, P. W. Davis, R. D. Graft, and T. S. Shilliday, "Radiation Effects in GaAs", J. Appl. Phys., vol. 34, p. 3590, 1963.

14. G. E. Brehm and G. L. Pearson, "Gamma-Radiation Damage in Epitaxial Gallium Arsenide", J. Appl. Phys., vol. 43, p. 568, 1972.

15. A. H. Kalma and R. A Berger, "Electrical Properties of Electron-Irradiated GaAs", IEEE Transactions on Nuclear Science, vol. NS-19, p. 167, 1972.

16. R. A. Berger, A. H. Kalma, and R. A. Cesena, "Electron-Irradiation of GaAs," International Conference on Defects in Semiconductions, p. 167, 1972.

17. M. U. Jeong, J. Shirafuji, and Y. Inuishi, "Radiation Effects in Semiconductors," Gordon and Breach Science Publishers, New York, p. 287, 1971.

18. H. J. Stein, "Electrical Studies of Low-Temperature Neutron- and Electron-Irradiated Epitaxial n-GaAs," J. Appl. Phys., vol. 40, p. 5300, 1969.

19. R. J. Mattauch, and M. P. Healy, "Electron-Irradiated Bulk n-Type GaAs," IEEE Transactions on Nuclear Science, vol. NS-22, p. 825, 1975.

20. Y. Yuba, K. Gamo, and S. Namba,"DLTS Study of Implanted GaAs," International Conference on Ion Beam Modification of Materials, Sept., 1978.

21. D. V. Lang, "Deep-Level Transient Spectroscopy: A New Method to Characterize Traps in Semiconductors," J. Applied Phys., vol. 45, p. 3023, 1974.

22. D. V. Lang, "Fast Capacitance Transient Apparatus: Application to ZnO and O Centers in GaP p-n Junctions," J. Applied Phys., vol. 45, p. 3015, 1974.

23. H. C. Casey, Jr., and M. B. Panish, "Composition Dependence of the $Ga_{1-x}Al_xAs$ Solar Cells with Multilayered Window Structure", IEEE Trans. on Electron Devices, vol. ED-25, p. 546, 1978.

24. A. Usami, Y. Hamamoto, and M. Sonobe, "A Computer Analysis of $Ga_{1-x}Al_xAs$-GaAs Solar Cells with Multilayered Window Structure", IEEE Trans. on Electron Devices, vol. #D-25, p. 546, 1978.

25. J. Lindhard, M. Scharff, H. E. Schitt, Kgl. Danske Vid. Selsk. Matt-Fys. Medd. 33, No. 14, 1963.

26. P. D. Townsend, J. C. Kelly, N. E. Hartly, "Ion Implantation, Sputtering and Their Applications", Academic Press, New York, p. 24, 1976.

27. S. Furukawa, H. Matsumura, and D. Ishiwara, "Theoretical Considerations on Lateral Spread of Implanted Ions", Japanese Jour. of Appl. Phys. vol 11, p. 134, 1972.

28. G. Dearnaley, J. H. Freeman, R. S. Nelson and J. Stephen, Ion Implantation, American Elsevier Publishing Co., Inc., p. 155, 1973.

29. S. W. Mylroie and J. F. Gibbons, "The Effect of Non-Gaussian Range Statistics on Energy Deposition Profiles", Ion Implantation in Semiconductors, edited by S. Namba, Plenum Press, New York, p. 413, 1974.

30. J. W. Mayer, L. Eriksson, and J. A. Davies, Ion Implantation in Semiconductors, Academic Press, New York, 1970.

31. C. T. Sah, R. N. Noyce, W. Shockley, "Carrier Generation and Recombination in P-N Junctions and P-N Junction Characteristics", Proc. of IRE, p. 1228, 1957.

32. W. Shockley and W. T. Read, "Statistics of the Recombinations of Holes and Electrons", Phys. Rev., 87, p. 835, 1952.

33. P. U. CalZolari, S. Graffi, "A Theoretical Investigation on the Generation Current in Silicon P-N Junctions under Reverse Bias", Solid-State Electronics, vol. 15, p. 1003, 1972.

34. C. T. Sah, "The Spatial Variation of the Quasi-Fermi Potentials", IEEE Trans. on Electron Devices, ED-13, p. 839, 1966.

35. A. E. Bakanowski and J. H. Forster, "Electrical Properties of Gold-Doped Diffused Silicon Computer Diodes", Bell System Tech. Jour., p. 87, 1960.

36. W. Shockley, "The Theory of P-N Junctions in Semiconductors and P-N Junction Transistors", Bell System Tech. Jour., vol. 28, p. 435, 1949.

37. A. R. Riben and D. L. Feucht, "N-Ge-P-GaAs Heterojunctions", Solid-State Electronics, vol. 9, p. 1055, 1966.

38. F. A. Lindholm, "Studies of Silicon PN Junction Solar Cells", Final Tech. Report, NASA NSG-3018, 1976.

39. R. J. Stirn, "Junction Characteristics of Silicon Solar Cells", NASA Tech. Memorandum 33-557, 1972.

40. M. Wolf, G. T Noel, and R. J. Stirn, "Investigation of the Double Exponential in the Current-Voltage Characteristics of Silicon Solar Cells", IEEE Trans. on Electron Devices, vol. ED-24, no. 4, 1977.

41. J. M. Andrews and M. P. Lepselter, "Reverse Current-Voltage Characteristics of Metal-Silicide Schottky Diodes", Solid-State Electronics, vol. 13, p. 1011, 1970.

42. R. A. Smith, Semiconductors, Cambridge at the University Press, 1959.

43. H. J. Hovel and J. M. Woodall, "Theoretical and Experimental Evaluation of $Ga_{1-x}Al_xAs$-GaAs Solar Cells", Solar Cells, IEEE Press, p. 288, 1976.

44. H. Harada and M. Fujimoto, "Electrical Properties of Proton Bombarded N-Type GaAs", Ion Implantation in Semiconductors, Plenum Press, p. 73, 1975.

45. F. Hasegawa, and A. Majerfeld, "Majority-Carrier Traps in n- and p-Type Epitaxial GaAs", Electronics Letters, vol. 11, p. 286, 1975.

46. K. Sakai, and T. Ikowa, "Deep Levels in GaAs by Capacitance Methods", Appl. Phys., vol. 5, p. 165, 1974.

47. C. I. Huang, and S. S. Li, "Analyses of Transient Capacitance Experiments for Au-GaAs Schottky Diodes in the Presence of Deep Impurities in the Interfacial Layer", Solid State Electron., vol. 16, p. 1481, 1973.

48. A. Mircea and A. Mitenneau, "Study of Electron Traps in Vapour-Phase Epitaxial GaAs", Appl. Phys., vol. 8, p. 15, 1975.

49. A. Ashby, G. G. Roberts, D. J. Ashen, and J. B. Mullin, "Nonextrinsic Condition in Semi-Insulating GaAs," Solid State Commun., vol. 20, p. 61, 1976.

50. D. V. Lang, and R. A. Logan, "A Study of Deep Levels in GaAs by Capacitance Spectroscopy", J. Electronic Mater., vol. 4, p. 1053, 1974.

51. D. V. Lang, A. Y. Cho, M. Ilegems, and W. Wiegmann, "Study of Electon Traps in n-GaAs Grown by Molecular Beam Epitaxy", J. Appl. Phys., vol. 47, p. 2558, 1970.

52. D. V. Lang, "Review of Radiation-Induced Defects in IV-V Compounds", Inst. Phys. Ser., no. 31, p. 70, 1977.

53. A. R. Kalma, R. A. Berger, and R. A Cesena, "Electron-Irradiation of GaAs", International Conf. on Defects in Semiconductors, p. 167, 1972.

54. N. J. Berg, and A. G. Lieberman., "The Effects of Radiation-Induced Displacement Damage on Impurity Conduction in Gallium Arsenide", J. Appl. Phys., vol. 46, p. 3475, 1975.

55. W. J. Brown, and J. S. Blakemore, "Transport and Photoelectrical Properties of Gallium Arsenide Containing Deep Acceptors", J. Appl. Phys., vol. 43, p. 2242, 1972.

56. L. L. Chang, L. Esaki and R. Tsu, "Vacancy Association of Defects in Annealed GaAs", Appl. Phys. Lett., vol. 19, p. 143, 1971.

57. G. E. Brehm and G. L. Pearson, "Gamma-Radiation Damage in Epitaxial Gallium Arsenide", J. Appl. Phys., vol. 43, p. 568, 1972.

58. A. H. Kalma, and R. A. Berger, "Electrical Properties of Electron-Irradiated GaAs", IEEE Transactions on Nuclear Science, vol. NS-19, p. 209, 1972.

59. A. R. Kalma, R. A. Berger, and R. A. Cesena, "Electron Irradiation of GaAs", International Conference on Defects in Semiconductors, p. 167, 1972.

60. M. U. Jeong, J. Shirafuji, and Y. Inuishi, Radiation Effects in Semiconductors, Gordon and Breach Science Publishers, New York, p. 287, 1971.

61. H. J. Stein, "Electrical Studies of Low-Temperature Neutron- and Electron-Irradiated Epitaxial n-Type GaAs", J. Appl. Phys., vol. 40, p. 5300, 1969.

62. L. W. Aukerman, P. W. Davis, R. D. Graft, and T. S. Shilliday, "Radiation Effects in GaAs", J. Appl. Phys., vol. 34, p. 3590, 1963.

63. K. Sakai, and T. Ikowa, "Deep Levels in GaAs by Capacitance Methods", Appl. Phys., vol. 5, p. 165, 1974.

64. A. Ashby, G. G. Roberts, D. J. Ashen and J. B. Mullin, "Non-Extrinsic Condition in Semi-Insulating GaAs", Solid State Commun., vol. 20, p. 61, 1976.

65. R. J. Mattauch, and M. P. Healy, "Electron-Irradiated Bulk n-Type GaAs", IEEE Transactions on Nuclear Science, vol. NS-22, p. 285, 1975.

66. D. V. Lang and L. C. Kimerling, "Observation of Recombination-Enhanced Defect Reactions in Semiconductors", Phys. Rev. Letters, vol. 33, p. 489, 1974.

67. Y. Yuba, K. Gamo, and S. Namba, "DLTS Study of Implanted GaAs", International Conf. on Ion Beam Modification of Materials, Sept., 1978.

68. D. V. Lang and C. H. Henry, "Nonradiative Recombination at Deep Levels in GaAs by Lattice-Relaxation Multiphonon Emission", Phys. Rev. Letters, vol. 35, p. 1525, 1975.

69. Y. Ikawa, A. Hojo, and M. Nakagawa, Japanese J. of Appl. Phys., vol. 17.1, 315, 1977.

70. A. G. Milnes, "Impurity and Defect Levels in GaAs," Advances in Electronics and Electron Physics, to be published 1981.

71. L. L. Chang, "Vacancy Association of Defects in Annealed GaAs," Appl. Phys. Lett., 19, p. 143, 1971.

72. W. E. Spicer, "Unified Defect Model and beyond," J. of Vac. Science Tech., 17 (5), p. 1019, 1980.

VIII. ACKNOWLEDGEMENT

In addition to Dr. Li, the principal investigator of this research project, Dr. D. W. Schoenfeld and several of Dr. Li's graduate students have made significant technical contributions during the course of this study. Dr. R. Y. Loo of Hughes Research Laboratories has fabricated all the AlGaAs-GaAs mesa diodes and performed the proton irradiation on all the samples used in this work. The collaboration of Dr. S. G. Kamath and R. Knechtli of Hughes Research Laboratories are also gratefully acknowledged. The author is also grateful to G. H. Walker of NASA Langley Research Center for his interest and support of this research project. The research was sponsored by NASA grant NSG-1425, Langley Research Center, Hampton, Virginia.